

Charm production from photo-nucleon reaction in a hadronic model

Wei Liu¹, Su Houng Lee^{1,2}, and Che Ming Ko¹

¹*Cyclotron Institute and Physics Department, Texas A&M University, College Station, Texas 77843-3366, USA*

²*Department of Physics and Institute of Physics and Applied Physics, Yonsei University, Seoul 120-749, Korea*

We study the total cross section for photo production of charmed hadrons near threshold using a hadronic Lagrangian. Both two-body final states involving Λ_c and a charmed meson as well as three-body final states involving nucleon and a charm-anticharm meson pair are included. With appropriate cut-off parameters in the form factors at interaction vertices, the model gives a total cross section that is consistent with the measured data at center-of-mass energy of 6 GeV. The result is compared with the prediction from the leading-order perturbative QCD.

PACS numbers: 25.75.-q, 13.75.Lb, 14.40.Gx, 14.40.Lb

I. INTRODUCTION

Reliable estimates of the production and scattering cross sections of open and/or hidden charmed hadrons in hadronic matter are important for understanding many phenomena in relativistic heavy ion collisions and hadron-nucleus reactions. In particular, the dissociation cross sections of J/ψ by light meson or nucleon are directly related to the role of hadronic suppression of J/ψ production in heavy ion collisions [1,2], and have thus been a subject under active investigations. In the heavy charm quark mass limit, a formula based on the leading-order (LO) perturbative QCD was derived in Refs. [3,4] for the absorption cross sections of J/ψ by hadrons. Higher-order corrections due to the target mass and relativistic effects have also been estimated [5–7]. However, the perturbative QCD approach is useful only at very high energy when nontrivial higher twist and higher α_s corrections are small. At low energies, these corrections become large, so nonperturbative approaches are needed. Various phenomenological models have thus been introduced for studying the J/ψ absorption cross section by hadrons at low energies. These include the hadronic model based on effective Lagrangians [8–10], the QCD sum rules [11], and the quark-exchange model [12]. Results from these phenomenological models all give much larger cross sections for J/ψ absorption by light mesons than that given by the perturbative QCD formula. To test the prediction from the hadronic model, the same effective Lagrangian has been used to evaluate the absorption cross section of J/ψ by nucleon, and it is found to be consistent with that extracted from photonuclear production of J/ψ [9].

In the present paper, we generalize the effective hadronic Lagrangian, which has also been used to study charmed meson scattering by hadrons [13,14] and charmed meson production from meson-nucleon scattering [15], to include the photon and to study charmed hadron production from photo-nucleon reaction near threshold. Both two-body ($\Lambda_c D$) and three-body ($N D \bar{D}$) final states are included. We find that using reasonable values for the cutoff parameters at the interaction vertices, the resulting charmed hadron production cross

section near threshold energy is consistent with the measured one at center-of-mass energy of 6 GeV [16], although at high energies its value is much smaller than that measured experimentally or given by the LO perturbative QCD. We further find that the relative contribution of two-body to three-body final states is also consistent with the experimental data. Our results thus provide another independent test and confirmation of the validity of hadronic model for determining the cross sections involving heavy flavors at low energies. The effective hadronic Lagrangian used in the present study will also be useful for evaluating other low energy cross sections involving heavy flavored hadrons, which can be studied at both the Japanese Hadron facility [17] and at the GSI future accelerator [18], where open and hidden charmed hadrons are copiously produced in proton- and antiproton-nucleus reactions near threshold.

This paper is organized as follows. In Section II, we first calculate the cross sections for photoproduction of charmed hadrons from nucleon with three particles in the final state, which is dominated by pion and rho meson exchange. Photoproduction of charmed hadrons from nucleon with two particle in the final state, which includes the charmed meson exchange, is studied in Section III. In Section IV, we show the total cross section and compare it to available experimental data and results from the LO QCD. Finally, summary and discussions are given in Section V.

II. PHOTOPRODUCTION OF CHARMED HADRONS FROM NUCLEON WITH THREE-PARTICLE FINAL STATES

In photoproduction of charmed hadrons from nucleon with three particle in the final states, the three possible reactions are $\gamma N \rightarrow \bar{D} D N$, $\gamma N \rightarrow \bar{D} D^* N (\bar{D}^* D N)$, and $\gamma N \rightarrow \bar{D}^* D^* N$. The lowest-order diagrams for the process $\gamma N \rightarrow \bar{D} D N$ are shown in Fig. 1 and involves the exchange of pion in the intermediate state; those for the processes $\gamma N \rightarrow \bar{D} D^* N (\bar{D}^* D N)$ and $\gamma N \rightarrow \bar{D}^* D^* N$ involve the exchange of rho meson, and the lowest-order diagrams for the two processes are shown in 2 and 3.

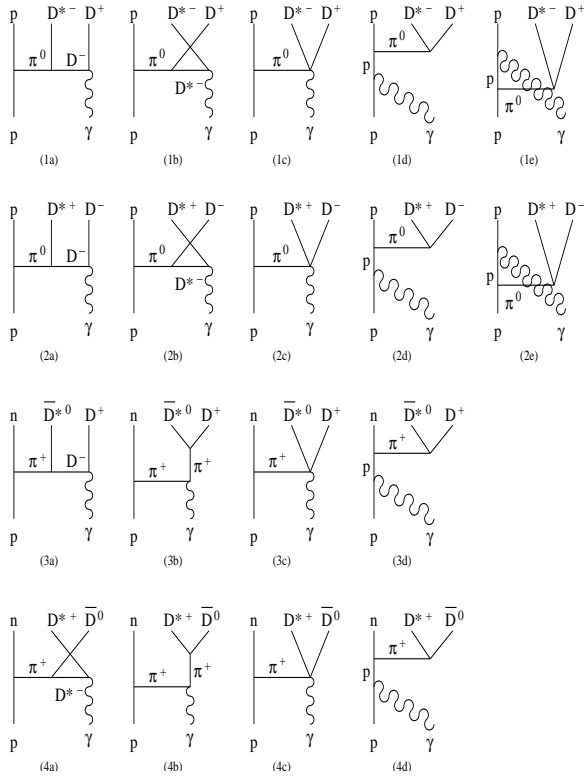


FIG. 1. Photoproduction of charmed hadrons from nucleon involving pion exchange.

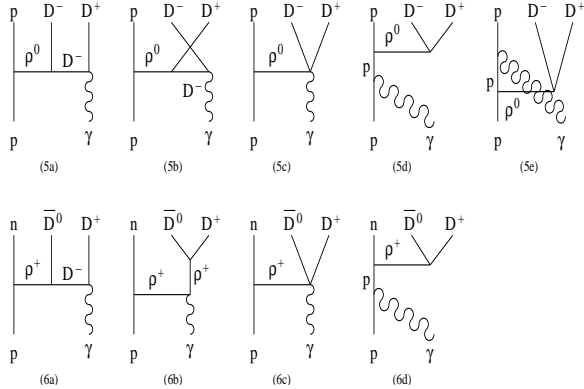


FIG. 2. Photoproduction of charmed hadrons ($D\bar{D}$) from proton involving rho meson exchange.

To evaluate the cross sections for these processes, we use the same Lagrangian introduced in Refs. [9,14,15] for studying charmed meson scattering by hadrons. This Lagrangian is based on the gauged SU(4) flavor symmetry but with empirical masses. The coupling constants are taken, if possible, from empirical information. Otherwise, the SU(4) relations are used to relate the unknown coupling constants to the known ones. Photon is then introduced in the Lagrangian via gauging its $U_{em}(1)$ part as in ref. [19].

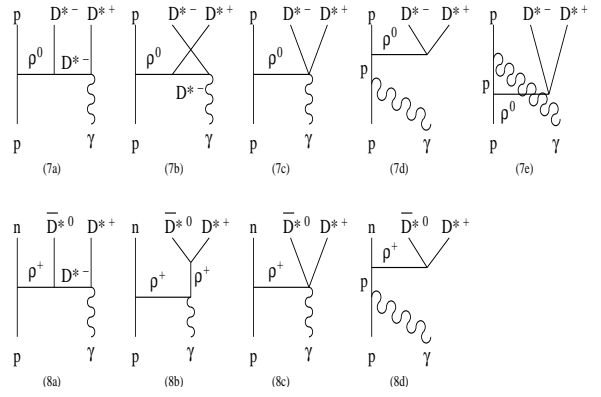


FIG. 3. Photoproduction of charmed hadrons ($D^* \bar{D}^*$) from proton involving rho meson exchange.

The interaction Lagrangian densities that are relevant to the processes shown in Figs. 1, 2, and 3 are given as follows:

$$\begin{aligned}
\mathcal{L}_{\pi NN} &= -ig_{\pi NN} \bar{N} \gamma_5 \vec{\tau} N \cdot \vec{\pi}, \\
\mathcal{L}_{\rho NN} &= g_{\rho NN} \bar{N} \left(\gamma^\mu \vec{\tau} \cdot \vec{\rho}_\mu + \frac{\kappa_\rho}{2m_N} \sigma_{\mu\nu} \vec{\tau} \cdot \partial_\mu \vec{\rho}_\nu \right) N, \\
\mathcal{L}_{\pi DD^*} &= ig_{\pi DD^*} D^{*\mu} \vec{\tau} \cdot (\bar{D} \partial_\mu \vec{\pi} - \partial_\mu \bar{D} \vec{\pi}) + \text{H.c.}, \\
\mathcal{L}_{\rho DD} &= ig_{\rho DD} (D \vec{\tau} \partial_\mu \bar{D} - \partial_\mu D \vec{\tau} \bar{D}) \cdot \vec{\rho}^\mu, \\
\mathcal{L}_{\rho D^* D^*} &= ig_{\rho D^* D^*} [(D_\mu D^{*\nu} \vec{\tau} \bar{D}_\nu^* - D^{*\nu} \vec{\tau} \partial_\mu \bar{D}_\nu^*) \cdot \vec{\rho}^\mu \\
&\quad + (D^{*\nu} \vec{\tau} \cdot \partial_\mu \vec{\rho}^\nu - \partial_\mu D^{*\nu} \vec{\tau} \cdot \vec{\rho}_\nu) \bar{D}^{*\mu} \\
&\quad + D^{*\mu} (\vec{\tau} \cdot \vec{\rho}^\nu \partial_\mu \bar{D}_\nu^* - \vec{\tau} \cdot \partial_\mu \vec{\rho}^\nu \bar{D}_\nu^*)], \\
\mathcal{L}_{\gamma DD} &= ieA^\mu [D Q \partial_\mu \bar{D} - (\partial_\mu D) Q \bar{D}], \\
\mathcal{L}_{\gamma D^* D^*} &= ie[A^\mu (\partial_\mu D^{*\nu} Q \bar{D}_\nu^* - D^{*\nu} Q \partial_\mu \bar{D}_\nu^*) \\
&\quad + (\partial_\mu A^\nu D_\nu^* - A^\nu \partial_\mu D_\nu^*) Q \bar{D}^{*\mu} \\
&\quad + D^{*\mu} Q (A^\nu \partial_\mu \bar{D}_\nu^* - \partial_\mu A^\nu \bar{D}_\nu^*)], \\
\mathcal{L}_{\pi \gamma DD^*} &= -eg_{\pi DD^*} A^\mu (D_\mu^* (2\vec{\tau} Q - Q \vec{\tau}) \bar{D} \\
&\quad + D (2Q \vec{\tau} - \vec{\tau} Q) \bar{D}_\mu^*) \cdot \vec{\pi}, \\
\mathcal{L}_{\rho \gamma DD} &= eg_{\rho DD} A^\mu D (\vec{\tau} Q + Q \vec{\tau}) \bar{D} \cdot \vec{\rho}_\mu, \\
\mathcal{L}_{\rho \gamma D^* D^*} &= eg_{\rho D^* D^*} (A^\nu D_\nu^* (2\vec{\tau} Q - Q \vec{\tau}) \bar{D}_\mu^* \\
&\quad + A^\nu D_\mu^* (2\vec{\tau} Q - Q \vec{\tau}) \bar{D}_\nu^* \\
&\quad - A_\mu D^{*\nu} (2\vec{\tau} Q - Q \vec{\tau}) \bar{D}_\nu^*) \cdot \vec{\rho}^\mu. \tag{1}
\end{aligned}$$

In the above, $\vec{\tau}$ are Pauli spin matrices, and $\vec{\pi}$ and $\vec{\rho}$ denote the pion and rho meson isospin triplet, respectively, while $D = (D^0, D^+)$ and $D^* = (D^{*0}, D^{*+})$ denote the pseudoscalar and vector charm meson doublets, respectively. The operator Q is the diagonal charge operator with diagonal elements equal to 0 and -1.

For coupling constants in the above interaction Lagrangians, we use the following empirical values: $g_{\pi NN} = 13.5$ [20], $g_{\rho NN} = 3.25$, $\kappa_\rho = 6.1$ [21], $g_{\pi DD^*} = 5.56$ [15,22], and $g_{\rho DD} = 2.52$ [14].

The diagrams in Figs. 1, 2, and 3 can be separated to two types; one in which the photon is coupled to mesons such as the first three diagrams (denoted by (ia) to (ic) with $i=1$ to 8), and the other in which the photon is

coupled directly to the incoming or outgoing charged nucleon. As shown later, contributions from the latter type are much smaller than those from the first type of diagrams and are thus neglected in the following calculations. We note that diagrams of the first type are similar to those for J/ψ absorption on nucleon, which can be interpreted as absorption by the virtual pion and rho meson cloud of a nucleon. Here, they can be considered as charmed hadron production from the nucleon's virtual meson cloud.

The amplitudes for the four processes in Fig. 1 are given by

$$\mathcal{M}_i = -ia g_{\pi NN} \bar{N}(p_3) \gamma_5 N(p_1) \frac{1}{t - m_\pi^2} \times (M_{ia} + M_{ib} + M_{ic}), \quad (2)$$

with $i = 1$ to 4, while the amplitudes for the four processes in Fig. 2, 3 can be written as

$$\begin{aligned} \mathcal{M}_j &= a g_{\rho NN} \bar{N}(p_3) \left[\gamma^\mu + i \frac{\kappa_\rho}{2m_N} \sigma^{\alpha\mu} (p_1 - p_3)_\alpha \right] \\ &\times N(p_1) \left[-g_{\mu\nu} + \frac{(p_1 - p_3)_\mu (p_1 - p_3)_\nu}{m_\rho^2} \right] \\ &\times \frac{1}{t - m_\rho^2} (M_{ja}^\nu + M_{jb}^\nu + M_{jc}^\nu), \end{aligned} \quad (3)$$

with $j = 5$ to 8. In the above, p_1 and p_3 are four momenta of the initial and final nucleons, respectively. The coefficient a is, respectively, 1 and $\sqrt{2}$ for neutral and charged pion coupling to nucleon.

The three amplitudes M_{ia} , M_{ib} , and M_{ic} are for the subprocess $\pi\gamma \rightarrow D^* \bar{D}$ in Fig. 1. It can be shown that they fulfill the chiral constraint [10], i.e., their sum vanishes at the soft pion limit. Explicitly, they are given by

$$\begin{aligned} \mathcal{M}_{1a} &= \mathcal{M}_{2a} \\ &= e g_{\pi DD^*} (-2k_1 + k_3)^\mu \frac{1}{t - m_D^2} \\ &\times (k_1 - k_3 + k_4)^\nu \varepsilon_{3\mu} \varepsilon_{2\nu}, \\ \mathcal{M}_{1b} &= \mathcal{M}_{2b} \\ &= -e g_{\pi DD^*} (-k_1 - k_4)^\alpha \frac{1}{u - m_{D^*}^2} \\ &\times \left[g_{\alpha\beta} - \frac{(k_1 - k_4)_\alpha (k_1 - k_4)_\beta}{m_{D^*}^2} \right] \\ &\times [(-k_2 - k_3)^\beta g^{\mu\nu} + (-k_1 + k_2 + k_4)^\nu g^{\beta\mu} \\ &+ (k_1 + k_3 - k_4)^\mu g^{\beta\nu}] \varepsilon_{3\mu} \varepsilon_{2\nu}, \\ \mathcal{M}_{1c} &= \mathcal{M}_{2c} \\ &= e g_{\pi DD^*} g^{\mu\nu} \varepsilon_{3\mu} \varepsilon_{2\nu}, \\ \mathcal{M}_{3a} &= \sqrt{2} e g_{\pi DD^*} (-2k_1 + k_3)^\mu \frac{1}{t - m_D^2} \\ &\times (k_1 - k_3 + k_4)^\nu \varepsilon_{3\mu} \varepsilon_{2\nu}, \\ \mathcal{M}_{3b} &= -\sqrt{2} e g_{\pi DD^*} (2k_1 + k_2)^\nu \frac{1}{s - m_\pi^2} \end{aligned}$$

$$\begin{aligned} &\times (k_1 + k_2 + k_4)^\mu \varepsilon_{3\mu} \varepsilon_{2\nu}, \\ \mathcal{M}_{3c} &= 2\sqrt{2} e g_{\pi DD^*} g^{\mu\nu} \varepsilon_{3\mu} \varepsilon_{2\nu}, \\ \mathcal{M}_{4a} &= -\sqrt{2} e g_{\pi DD^*} (-k_1 - k_4)^\alpha \frac{1}{u - m_{D^*}^2} \\ &\times \left[g_{\alpha\beta} - \frac{(k_1 - k_4)_\alpha (k_1 - k_4)_\beta}{m_{D^*}^2} \right] \\ &\times [(-k_2 - k_3)^\beta g^{\mu\nu} + (-k_1 + k_2 + k_4)^\nu g^{\beta\mu} \\ &+ (k_1 + k_3 - k_4)^\mu g^{\beta\nu}] \varepsilon_{3\mu} \varepsilon_{2\nu}, \\ \mathcal{M}_{4b} &= \sqrt{2} e g_{\pi DD^*} (2k_1 + k_2)^\nu \frac{1}{s - m_\pi^2} \\ &\times (k_1 + k_2 + k_4)^\mu \varepsilon_{3\mu} \varepsilon_{2\nu}, \\ \mathcal{M}_{4c} &= -\sqrt{2} e g_{\pi DD^*} g^{\mu\nu} \varepsilon_{3\mu} \varepsilon_{2\nu}, \end{aligned} \quad (4)$$

where k_i denotes the momentum of particle i of each subprocess, and ε_μ and ε_ν are the polarization vector of γ and D^* , respectively. We choose the convention that particles 1 and 2 represent initial-state particles while particles 3 and 4 represent final-state ones on the left and right sides of the diagrams.

The amplitudes M_{ja}^ν , M_{jb}^ν , and M_{jc}^ν are those for the subprocesses $\rho\gamma \rightarrow D\bar{D}$ and $\rho\gamma \rightarrow D^* \bar{D}^*$ in Figs. 2 and 3, and they are written explicitly as:

$$\begin{aligned} \mathcal{M}_{5a}^\mu &= -e g_{\rho DD} (k_1 - 2k_3)^\mu \frac{1}{t - m_D^2} \\ &\times (k_1 - k_3 + k_4)^\nu \varepsilon_{2\nu}, \\ \mathcal{M}_{5b}^\mu &= -e g_{\rho DD} (-k_1 + 2k_4)^\mu \frac{1}{u - m_D^2} \\ &\times (-k_1 - k_3 + k_4)^\nu \varepsilon_{2\nu}, \\ \mathcal{M}_{5c}^\mu &= 2e g_{\rho DD} g^{\mu\nu} \varepsilon_{2\nu}, \\ \mathcal{M}_{6a}^\mu &= \sqrt{2} e g_{\rho DD} (k_1 - 2k_3)^\mu \frac{1}{t - m_D^2} \\ &\times (k_1 - k_3 + k_4)^\nu \varepsilon_{2\nu}, \\ \mathcal{M}_{6b}^\mu &= \sqrt{2} e g_{\rho DD} [(-2k_1 - k_2)^\nu g^{\mu\alpha} \\ &+ (k_1 + 2k_2)^\mu g^{\alpha\nu} + (k_1 - k_2)^\alpha g^{\mu\nu}] \frac{1}{s - m_\rho^2} \\ &\times \left[g_{\alpha\beta} - \frac{(k_1 + k_2)_\alpha (k_1 + k_2)_\beta}{m_\rho^2} \right] \\ &\times (k_3 - k_4)^\beta \varepsilon_{2\nu}, \\ \mathcal{M}_{6c}^\mu &= -\sqrt{2} e g_{\rho DD} g^{\mu\nu} \varepsilon_{2\nu}, \\ \mathcal{M}_{7a}^\mu &= e g_{\rho D^* D^*} [(-k_1 - k_3)^\alpha g^{\mu\lambda} + (2k_1 - k_3)^\lambda g^{\alpha\mu} \\ &+ (2k_3 - k_1)^\mu g^{\alpha\lambda}] \frac{1}{t - m_{D^*}^2} \\ &\times \left[g_{\alpha\beta} - \frac{(k_1 - k_3)_\alpha (k_1 - k_3)_\beta}{m_{D^*}^2} \right] \\ &\times [-2p_2^\omega g^{\beta\nu} + (k_2 + k_4)^\beta g^{\nu\omega} - 2k_4^\nu g^{\beta\omega}] \\ &\times \varepsilon_{2\nu} \varepsilon_{3\lambda} \varepsilon_{4\omega}, \\ \mathcal{M}_{7b}^\mu &= e g_{\rho D^* D^*} [(-2k_1 + k_4)^\omega g^{\alpha\mu} + (k_1 + k_4)^\alpha g^{\mu\omega} \end{aligned}$$

$$\begin{aligned}
& + (k_1 - 2k_4)^\mu g^{\alpha\omega}] \frac{1}{u - m_{D^*}^2} \\
& \times \left[g_{\alpha\beta} - \frac{(k_1 - k_4)_\alpha (k_1 - k_4)_\beta}{m_{D^*}^2} \right] \\
& \times [(-k_2 - k_3)^\beta g^{\nu\lambda} + 2k_2^\lambda g^{\beta\nu} + 2k_3^\nu g^{\beta\lambda}] \\
& \times \varepsilon_{2\nu} \varepsilon_{3\lambda} \varepsilon_{4\omega}, \\
\mathcal{M}_{7c}^\mu & = eg_{\rho D^* D^*} (g^{\mu\lambda} g^{\nu\omega} + g^{\mu\omega} g^{\nu\lambda} - 2g^{\mu\nu} g^{\lambda\omega}) \\
& \times \varepsilon_{2\nu} \varepsilon_{3\lambda} \varepsilon_{4\omega}, \\
\mathcal{M}_{8a}^\mu & = \sqrt{2} eg_{\rho D^* D^*} [(-k_1 - k_3)^\alpha g^{\mu\lambda} + (2p_1 - p_3)^\lambda g^{\alpha\mu} \\
& + (2k_3 - k_1)^\mu g^{\alpha\lambda}] \frac{1}{t - m_{D^*}^2} \\
& \times \left[g_{\alpha\beta} - \frac{(k_1 - k_3)_\alpha (k_1 - k_3)_\beta}{m_{D^*}^2} \right] \\
& \times [-2p_2^\omega g^{\beta\nu} + (k_2 + k_4)^\beta g^{\nu\omega} - 2k_4^\nu g^{\beta\omega}] \\
& \times \varepsilon_{2\nu} \varepsilon_{3\lambda} \varepsilon_{4\omega}, \\
\mathcal{M}_{8b}^\mu & = -\sqrt{2} eg_{\rho D^* D^*} [(-2k_1 - k_2)^\nu g^{\mu\alpha} + (k_1 + 2k_2)^\mu g^{\alpha\nu} \\
& + (k_1 - k_2)^\alpha g^{\mu\nu}] \frac{1}{s - m_\rho^2} \\
& \times \left[g_{\alpha\beta} - \frac{(k_1 + k_2)_\alpha (k_1 + k_2)_\beta}{m_\rho^2} \right] \\
& \times [-2k_4^\lambda g^{\beta\omega} + 2k_3^\omega g^{\beta\lambda} + (k_4 - k_3)^\beta g^{\lambda\omega}] \\
& \times \varepsilon_{2\nu} \varepsilon_{3\lambda} \varepsilon_{4\omega}, \\
\mathcal{M}_{8c}^\mu & = -\sqrt{2} eg_{\rho D^* D^*} (g^{\mu\lambda} g^{\nu\omega} - 2g^{\mu\omega} g^{\nu\lambda} + g^{\mu\nu} g^{\lambda\omega}) \\
& \times \varepsilon_{2\nu} \varepsilon_{3\lambda} \varepsilon_{4\omega}. \tag{5}
\end{aligned}$$

The cross sections for these reactions with three particles in the final state can be expressed in terms of the off-shell cross sections of the subprocesses involving two particles in the final state. Following the method of Ref. [23] for the reaction $NN \rightarrow N\Lambda K$, the spin-averaged differential cross section for the four reactions in Fig. 1 can be written as

$$\begin{aligned}
\frac{d\sigma_{\gamma N \rightarrow ND^* \bar{D}}}{dtds_1} & = \frac{ag_{\pi NN}^2}{32\pi^2 sp_c^2} k\sqrt{s_1}(-t) \frac{1}{(t - m_\pi^2)^2} \\
& \times \sigma_{\rho\gamma \rightarrow D^* \bar{D}}(s_1, t) |F(t)|^2, \tag{6}
\end{aligned}$$

while those for the two reactions in Fig. 2 are

$$\begin{aligned}
\frac{d\sigma_{\gamma N \rightarrow ND \bar{D}}}{dtds_1} & = \frac{3ag_{\rho NN}^2}{64\pi^2 sp_c^2} k\sqrt{s_1} \frac{1}{(t - m_\rho^2)^2} [4(1 + \kappa_\rho)^2 \\
& \times (-t - 2m_N^2) \kappa_\rho^2 \frac{(4m_N^2 - t)^2}{2m_N^2} + 4(1 + \kappa_\rho) \\
& \times \kappa_\rho(4m_N^2 - t)] \sigma_{\rho\gamma \rightarrow D \bar{D}}(s_1, t) |F(t)|^2. \tag{7}
\end{aligned}$$

In the above, p_c is the center-of-mass momentum of γ and N , t is the squared four momentum transfer, and s is the squared center-of-mass energy. The quantity s_1 and k are, respectively, the squared invariant mass and center-of-mass momentum of the π and γ in the subprocess $\gamma N \rightarrow D^* \bar{D} N$ or of the ρ and γ in the subprocesses

$\gamma N \rightarrow D \bar{D} N$ and $\gamma N \rightarrow D^* \bar{D}^* N$. Cross sections for these subprocesses are obtained from the amplitudes in Eqs.(4) and (5) using the software package FORM [24] to evaluate the summation over the polarizations of both initial and final particles. The differential cross sections for the two reactions $\gamma N \rightarrow D^* \bar{D}^* N$ in Fig. 3 are similar to those for $\gamma N \rightarrow D \bar{D} N$ with $\sigma_{\rho\gamma \rightarrow D \bar{D}}(s_1, t)$ replaced by $\sigma_{\rho\gamma \rightarrow D^* \bar{D}^*}(s_1, t)$.

We have introduced the form factors $F_{\pi NN}$ and $F_{\rho NN}$ at the πNN and ρNN vertices, respectively, to take into account the finite size of hadrons. As in Ref. [9], both are taken to have the following monopole form:

$$F(t) = \frac{\Lambda^2 - m^2}{\Lambda^2 - t}, \tag{8}$$

where m is the mass of the exchanged pion or rho meson, and Λ is a cutoff parameter. Following Ref. [9] we take $\Lambda_{\pi NN} = 1.3$ GeV and $\Lambda_{\rho NN} = 1.4$ GeV. We have also introduced a universal form factor at the strong interaction vertices in the $\pi\gamma \rightarrow D^* D$, $\rho\gamma \rightarrow DD$, and $\rho\gamma \rightarrow D^* D^*$ two-body subprocesses. Such a prescription guarantees the gauge invariance when all diagrams are included in each process [25]. The form factor we include here is of the following dipole form:

$$f(\mathbf{q}^2) = \left(\frac{\Lambda^2}{\Lambda^2 + \mathbf{q}^2} \right)^2, \tag{9}$$

with \mathbf{q} denoting the three momentum of photon in the center-of-mass system. We choose the cutoff parameter Λ to be 1.45 GeV to best reproduce the data. This form is also our default choice of form factors in this paper, unless stated otherwise.

The cross sections for charmed hadron production from neutron is the same as that from proton if we neglect diagrams involving photon coupling directly to proton. The isospin-averaged cross section for the reaction $\gamma N \rightarrow \bar{D} D N$ is thus given by the sum of the cross sections for the four processes in Fig. 1, which are obtained by integrating Eq.(6) over t and s_1 . Similarly, one can obtain from Eq.(7) the isospin averaged cross sections for the reactions $\gamma N \rightarrow \bar{D} D^* N(\bar{D}^* D N)$ and $\gamma N \rightarrow \bar{D}^* D^* N$, shown respectively, in Figs. 2 and 3. The results are shown in Fig. 4 by the solid, dotted, and dashed curves, respectively, for the reactions $\gamma N \rightarrow \bar{D} D N$, $\gamma N \rightarrow \bar{D} D^* N(\bar{D}^* D N)$ and $\gamma N \rightarrow \bar{D}^* D^* N$. It is seen that the reaction $\gamma N \rightarrow \bar{D} D^* N(\bar{D}^* D N)$ has the largest cross section with a peak value of about 40 nb, while the reaction $\gamma N \rightarrow \bar{D} D N$ has the smallest cross section of only about 1 nb. The larger cross sections for processes involving a charmed vector meson in the final state is due to the presence of interaction vertices with three vector mesons, which have a stronger momentum dependence than vertices with fewer number of vector mesons, leading thus to a larger strength at high energies.

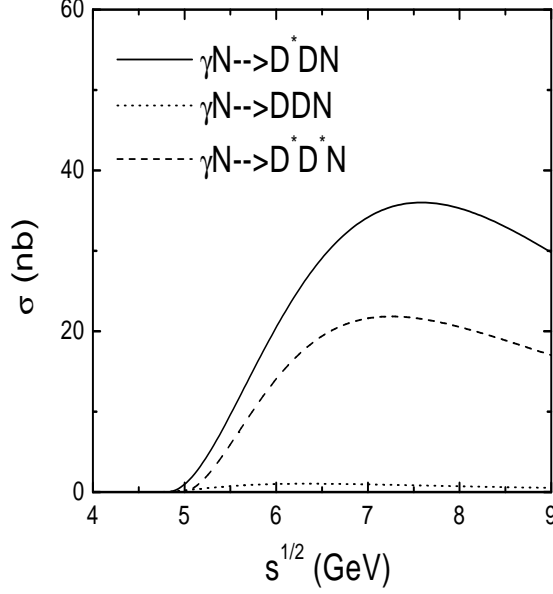


FIG. 4. Cross sections for photoproduction of charmed hadrons from nucleon with three particles in the final states.

The above results are obtained without contributions from diagrams involving the photon coupled directly to external nucleons. These diagrams are needed to preserve the gauge invariance in each process. Their contributions are small compared to those from diagrams with the photon coupled directly to mesons. This is due to the s -channel nucleon propagator ($1/(s - m_N^2)$) in these diagrams, which suppresses their amplitudes more than the t -channel heavy meson propagator in other as a result of the large photon energy needed to produce both the charmed and anticharmed meson pair. In the following, we demonstrate this effect by comparing the contribution due to diagram (1d) with that due to diagrams (1a)-(1c) in Fig. 1.

The amplitude for diagram (1d) in Fig. 1 can be written as

$$\begin{aligned} \mathcal{M} &= i2eg_{\pi NN}g_{\pi DD^*} \frac{1}{(s - m_N^2)(t - m_\pi^2)} \\ &\times \bar{p}(p_3)\gamma_5(\not{p}_1 + \not{p}_2 + m_N)\gamma^\mu p(p_1)\varepsilon_\mu p_5^\nu \varepsilon_\nu \\ &\equiv 2g_{\pi DD^*}M_2 p_5^\nu \varepsilon_\nu, \end{aligned} \quad (10)$$

where p_1 , p_3 , p_2 , and p_5 are the momenta of initial and final nucleons, photon, and charmed meson, respectively. The cross section due to this diagram alone is given by

$$\frac{d\sigma}{dtds_1} = \frac{\sqrt{s_1}}{256\pi^2 s p_c^2} |\mathcal{M}_2|^2 \Gamma(s_1), \quad (11)$$

where again p_c is the center-of-mass momentum of the nucleon and the photon, s_1 is the invariant mass of the $D^{*-}D^+$ pair, and $\Gamma(s_1)$ is the decay width of the off-shell $\pi^0 \rightarrow D^{*-}D^+$.

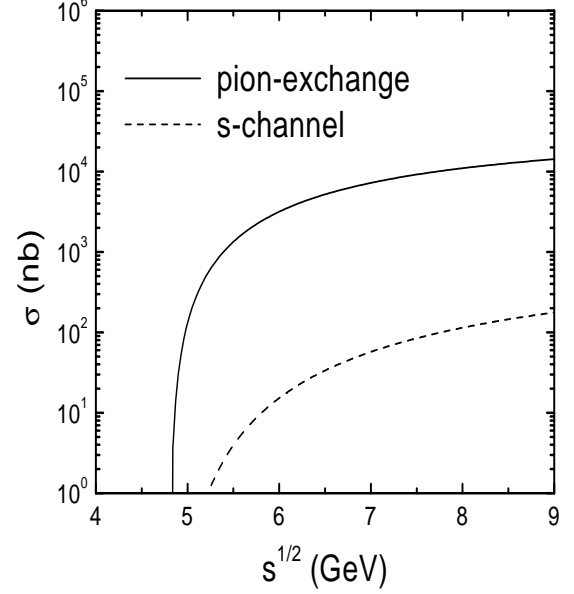


FIG. 5. Cross sections due to photon coupling directly to nucleon (diagram (1d) in Fig. 1, dashed curve) and due to pion exchange (diagrams (1a)-(1c) in Fig. 1, solid curve). No form factors are included at interaction vertices.

The cross section due to the s -channel diagram (1d) in Fig. 1 involving photon coupling directly to nucleon is shown by the dashed curve in Fig. 5 together with that coming from the pion exchange contributions (diagrams (1a)-(1c) in Fig. 1), shown by the solid curve. Form factors have been neglected in these results as we are only interested in their relative magnitude. It is seen that the contribution from the diagram with direct photon-nucleon coupling is more than two orders of magnitude smaller than that from the pion-exchange diagrams and can thus be safely neglected.

III. PHOTOPRODUCTION OF CHARMED HADRONS FROM NUCLEON WITH TWO-BODY FINAL STATES

Charmed hadron can also be produced in photon-nucleon reaction from processes involving two particles in the final state, i.e., $\gamma N \rightarrow \bar{D}\Lambda_c$ and $\gamma N \rightarrow \bar{D}^*\Lambda_c$, shown by diagrams in Fig. 6. The interaction Lagrangians needed to evaluate the cross sections for these reactions are:

$$\begin{aligned} \mathcal{L}_{DN\Lambda_c} &= ig_{DN\Lambda_c}(\bar{N}\gamma_5\Lambda_c\bar{D} + D\bar{\Lambda}_c\gamma_5 N), \\ \mathcal{L}_{D^*N\Lambda_c} &= g_{D^*N\Lambda_c}(\bar{N}\gamma_\mu\Lambda_c D^{*\mu} + \bar{D}^{*\mu}\bar{\Lambda}_c\gamma_\mu N). \end{aligned} \quad (12)$$

As in ref. [15], we use SU(4) relations to determine the coupling constants $g_{DN\Lambda_c}$ and $g_{D^*N\Lambda_c}$ in terms of known

coupling constants $g_{\pi NN}$ and $g_{\rho NN}$, and they are given by

$$g_{D N \Lambda_c} = \frac{3 - 2\alpha_D}{\sqrt{3}} g_{\pi NN} \simeq g_{\pi NN} = 13.5, \\ g_{D^* N \Lambda_c} = -\sqrt{3} g_{\rho NN} = -5.6, \quad (13)$$

where $\alpha_D = D/(D + F) \simeq 0.64$ [26] with D and F being the coefficients for the usual D -type and F -type couplings. Values of these couplings constants are similar to those obtained from a QCD sum rule analysis [27].

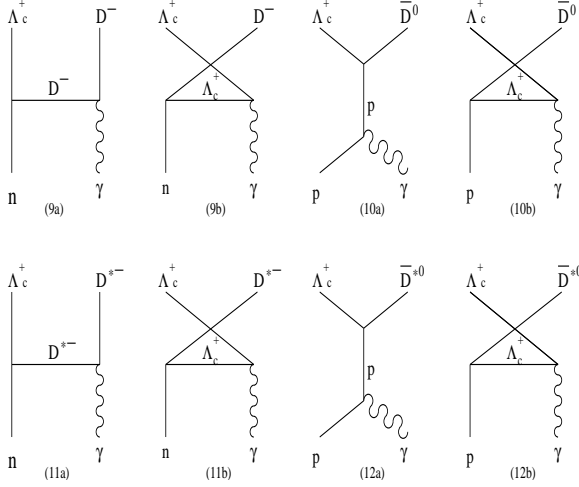


FIG. 6. Photoproduction of charmed hadrons from nucleon with two-particle final states.

The amplitudes for the two processes in Fig. 6 are

$$\begin{aligned} \mathcal{M}_9 &= (\mathcal{M}_{9a}^\mu + \mathcal{M}_{9b}^\mu) \varepsilon_\mu, \\ \mathcal{M}_{10} &= (\mathcal{M}_{10a}^\mu + \mathcal{M}_{10b}^\mu) \varepsilon_\mu, \\ \mathcal{M}_{11} &= (\mathcal{M}_{11a}^{\mu\nu} + \mathcal{M}_{11b}^{\mu\nu}) \varepsilon_\mu \varepsilon_\nu, \\ \mathcal{M}_{12} &= (\mathcal{M}_{12a}^{\mu\nu} + \mathcal{M}_{12b}^{\mu\nu}) \varepsilon_\mu \varepsilon_\nu, \end{aligned} \quad (14)$$

with \mathcal{M}_{9a}^μ , \mathcal{M}_{9b}^μ , \mathcal{M}_{10a}^μ , and \mathcal{M}_{10b}^μ for the top four diagrams in Fig. 6, while $\mathcal{M}_{11a}^{\mu\nu}$, $\mathcal{M}_{11b}^{\mu\nu}$, $\mathcal{M}_{12a}^{\mu\nu}$, and $\mathcal{M}_{12b}^{\mu\nu}$ for the bottom four diagrams. They are given explicitly by

$$\begin{aligned} \mathcal{M}_{9a}^\mu &= i e g_{D N \Lambda_c} \frac{1}{t - m_D^2} (p_2 - 2p_4)^\mu \bar{\Lambda}_c(p_3) \gamma^5 n(p_1), \\ \mathcal{M}_{9b}^\mu &= i e g_{D N \Lambda_c} \frac{1}{u - m_{\Lambda_c}^2} \\ &\quad \times \bar{\Lambda}_c(p_3) \gamma^\mu (\not{p}_1 - \not{p}_4 + m_{\Lambda_c}) \gamma^5 n(p_1), \\ \mathcal{M}_{10a}^\mu &= i e g_{D N \Lambda_c} \frac{1}{s - m_N^2} \\ &\quad \times \bar{\Lambda}_c(p_3) \gamma^5 (\not{p}_1 + \not{p}_2 + m_N) \gamma^\mu p(p_1), \\ \mathcal{M}_{10b}^\mu &= i e g_{D N \Lambda_c} \frac{1}{u - m_{\Lambda_c}^2} \\ &\quad \times \bar{\Lambda}_c(p_3) \gamma^\mu (\not{p}_1 - \not{p}_4 + m_{\Lambda_c}) \gamma^5 p(p_1), \end{aligned}$$

$$\begin{aligned} \mathcal{M}_{11a}^{\mu\nu} &= e g_{D^* N \Lambda_c} \bar{\Lambda}_c(p_3) \gamma^\alpha n(p_1) \frac{1}{t - m_{D^*}^2} \\ &\quad \times \left[-g_{\alpha\beta} + \frac{(p_1 - p_3)_\alpha (p_1 - p_3)_\beta}{m_{D^*}^2} \right] \\ &\quad \times [2p_2^\nu g^{\beta\mu} - (p_2 + p_4)^\beta g^{\mu\nu} + 2p_4^\mu g^{\beta\nu}], \\ \mathcal{M}_{11b}^{\mu\nu} &= e g_{D^* N \Lambda_c} \frac{1}{u - m_{\Lambda_c}^2} \\ &\quad \times \bar{\Lambda}_c(p_3) \gamma^\mu (\not{p}_1 - \not{p}_4 + m_{\Lambda_c}) \gamma^\nu n(p_1), \\ \mathcal{M}_{12a}^{\mu\nu} &= e g_{D^* N \Lambda_c} \frac{1}{s - m_N^2} \\ &\quad \times \bar{\Lambda}_c(p_3) \gamma^\nu (\not{p}_1 + \not{p}_2 + m_N) \gamma^\mu p(p_1), \\ \mathcal{M}_{12b}^{\mu\nu} &= e g_{D^* N \Lambda_c} \frac{1}{u - m_{\Lambda_c}^2} \\ &\quad \times \bar{\Lambda}_c(p_3) \gamma^\mu (\not{p}_1 - \not{p}_4 + m_{\Lambda_c}) \gamma^\nu p(p_1). \end{aligned} \quad (15)$$

Here, p_1 , p_2 , p_3 , and p_4 denote the momentum of γ , N , $\bar{D}(\bar{D}^*)$, and Λ_c , respectively.

The spin-averaged differential cross sections for the four processes in Fig. 6 are then

$$\frac{d\sigma_{\gamma N \rightarrow \bar{D} \Lambda_c}}{dt} = \frac{1}{256\pi s p_c^2} |\mathcal{M}_i|^2 |f(\mathbf{q}^2)|^2, \quad (16)$$

where $i = 9, 10, 11, 12$ for the the four reactions $\gamma n \rightarrow D^- \Lambda_c^+$, $\gamma p \rightarrow \bar{D}^0 \Lambda_c^+$, $\gamma n \rightarrow D^{*-} \Lambda_c^+$, and $\gamma \rightarrow D^- \Lambda_c^+$.

The isospin-averaged cross sections for the two reactions $\gamma N \rightarrow \bar{D} \Lambda_c$ and $\gamma N \rightarrow \bar{D}^* \Lambda_c$ can be obtained from the above cross sections, and they are given by

$$\begin{aligned} \sigma_{\gamma N \rightarrow \bar{D} \Lambda_c} &= \frac{1}{2} (\sigma_{\gamma n \rightarrow D^- \Lambda_c^+} + \sigma_{\gamma p \rightarrow \bar{D}^0 \Lambda_c^+}), \\ \sigma_{\gamma N \rightarrow \bar{D}^* \Lambda_c} &= \frac{1}{2} (\sigma_{\gamma n \rightarrow D^{*-} \Lambda_c^+} + \sigma_{\gamma p \rightarrow \bar{D}^{*0} \Lambda_c^+}). \end{aligned} \quad (17)$$

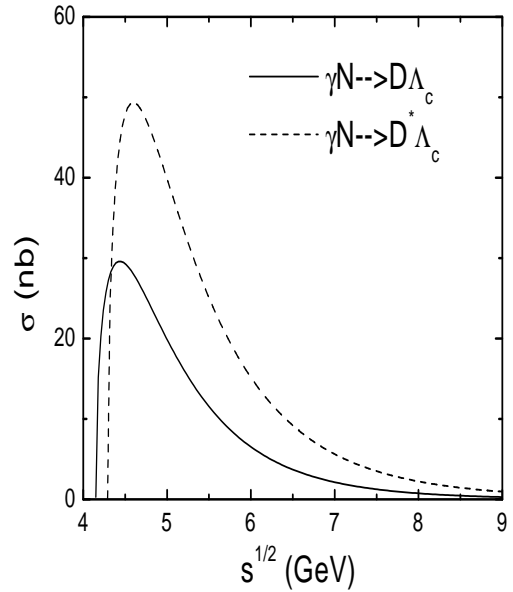


FIG. 7. cross section photoproduction of charmed hadrons via charmed meson exchange.

Taking the form factor at interaction vertices to be of the dipole type as in Eq. (9) and with a cutoff parameter $\Lambda = 1.45$ GeV, which is chosen to reproduce the experimentally observed relative strength between two-body and three-body decay final states in photoproduction of charmed hadrons on nucleon [16], the cross sections for the reactions $\gamma N \rightarrow \bar{D}\Lambda_c$ (dashed curve) and $\gamma N \rightarrow \bar{D}^*\Lambda_c$ (solid curve) are shown in Fig. 7 as functions of total center-of-mass energy. It is seen that both cross sections are large with a peak value of about 30 nb for $\gamma N \rightarrow \bar{D}\Lambda_c$ and about 50 nb for $\gamma N \rightarrow \bar{D}^*\Lambda_c$.

IV. TOTAL CROSS SECTION FOR CHARMED HADRON PRODUCTION IN PHOTON-NUCLEON REACTION

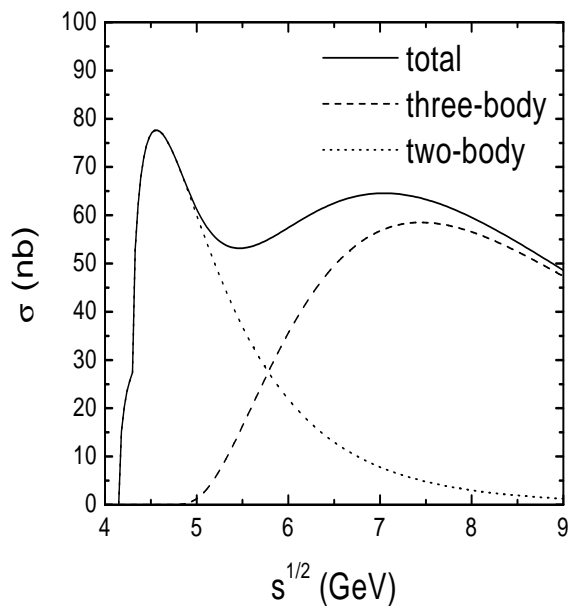


FIG. 8. Total and partial cross sections for charmed hadron production in photon-nucleon reactions as functions of center-of-mass energy.

The total cross section for photoproduction of charmed hadrons on nucleon is given by the sum of the cross sections for two-body and three-body final states. In Fig. 8, we show the total cross section (solid curve) together with that for two-body final state (dotted curve) and three-body final state (dashed curve). It is seen that two-body final states involving Λ_c and a charmed meson dominates at low energy, while the three-body final state involving a nucleon as well as a charmed and anticharmed meson pair is more important at high energies. The two have

comparable magnitudes around center-of-mass energy of about 5.7 GeV. This is consistent with the experimental data at 6 GeV [16], which shows that the final state with a Λ_c constitutes about 35% of the total cross section.

Charm production from photo-nucleon reaction can be estimated using the leading-order perturbative QCD [28–30]. The cross section in this approach is given by

$$\sigma^{\gamma N}(\nu) = \int_{2m_c^2/\nu}^1 dx \sigma^{\gamma g}(\nu x)g(x), \quad (18)$$

where m_c is the charm quark mass, $g(x)$ is the gluon distribution function inside the nucleon, and $\nu = p \cdot p_\gamma$ with p and p_γ being the momenta of the incoming nucleon and photon. The cross section $\sigma^{\gamma g}(\omega)$ is that for charm-anticharm quark production from the leading order photon-gluon scattering, i.e.,

$$\begin{aligned} \sigma^{\gamma g \rightarrow \bar{c}c}(\omega) = & \frac{2\pi\alpha_s\alpha}{9} \frac{4}{\omega^2} \left[\left(1 + \frac{4m_c^2}{\omega^2} - \frac{8m_c^2}{\omega^4} \right) \right. \\ & \times \log \frac{1 + \sqrt{1 - \frac{4m_c^2}{\omega^2}}}{1 + \sqrt{1 - \frac{4m_c^2}{\omega^2}}} \\ & \left. - \left(1 + \frac{4m_c^2}{\omega^2} \right) \sqrt{1 - \frac{4m_c^2}{\omega^2}} \right], \quad (19) \end{aligned}$$

where $\omega^2 = 2p_g \cdot p_\gamma$, with the gluon momentum denoted by p_g .

Using $m_c = 1.3$ GeV and the leading order MRST 2001 parameterization of the gluon distribution function in nucleon [31], we have calculated the photo charm production cross section on nucleon using the LO QCD formula, and the result is shown Fig. 9 by the dashed curve together with that from the effective hadronic model (solid curve) and the available experimental data (open circles). We see that the LO QCD result reproduces the data at 6 GeV and at higher energies. However, the QCD prediction below 6 GeV falls well below the results from the effective hadronic model. It is known that the QCD formula for photoproduction of heavy quarks should work best when the momenta involved are of order the heavy quark mass m_c . Below this momentum and near the threshold energy, large logarithms will appear in the perturbative QCD approach and spoil its convergence [32]. At these energies, our phenomenological hadronic approach should be more reliable as the cross section is dominated by two-body final states with no additional contribution to cause any large correction. On the other hand, the results from the hadronic model at higher energies fall short of the experimental data. This is expected because at these energies, contributions from four-body final state and from the exchange of heavier mesons will become important. At these higher energies, perturbative QCD calculations should be a more efficient way for determining the cross section for photo charm production than adding new ingredients into our phenomenological hadronic model.

ACKNOWLEDGMENT

This paper is based on work supported by the National Science Foundation under Grant No. PHY-0098805 and the Welch Foundation under Grant No. A-1358. SHL is also supported in part by the KOSEF under Grant No. 1999-2-111-005-5 and by the Korea Research Foundation under Grant No. KRF-2002-015-CP0074.

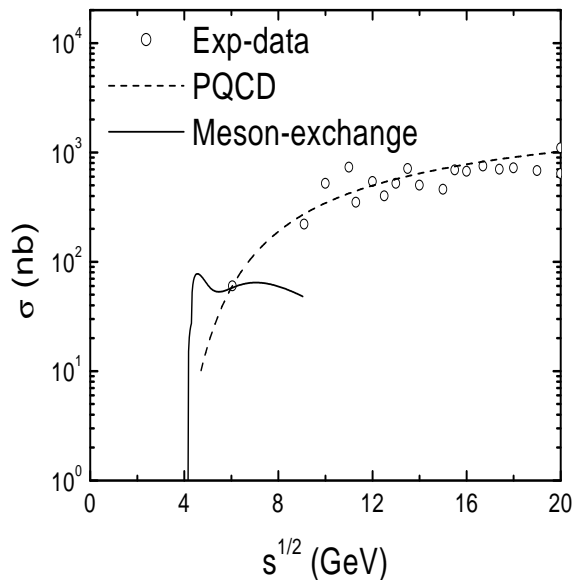


FIG. 9. Cross sections for charm production in photo nucleon reaction in the hadronic model (solid curve) and the pQCD approach (dashed curve). The experimental data are shown by open circles.

V. SUMMARY AND DISCUSSIONS

In summary, the total cross section for charmed hadron production in photo-nucleon reaction is evaluated in an effective hadronic model. This model is based on a gauged SU(4) flavor symmetric Lagrangian with the photon introduced as a $U_{em}(1)$ gauged particle. The symmetry breaking effect is taken into account via using empirical hadron masses and coupling constants. Form factors of the monopole type are introduced at interaction vertices. This hadronic model has been previously used to evaluate the dissociation cross section of J/ψ by hadrons. For photo production of charmed hadrons on nucleon, we have included both two-body final states involving a Λ_c and a charmed meson as well as three-body final states involving a nucleon and a charmed and anticharmed meson pair. It is found that reactions with two-body final states dominate the production cross section at low center-of-mass energies while reactions with three-body states are more important at high center-of-mass energies. Using cut-off parameters in the form factors from previous studies of J/ψ absorption by hadrons, the model reproduces the lowest available experimental data at center-of-mass energy of 6 GeV. Our results thus again confirm the validity of the effective hadron model in previous studies and provide a useful model for further studies of reactions involving heavy quarks at low and near threshold energies.

- [1] W. Cassing and C. M. Ko, Phys. Lett. B **396**, 39 (1997); W. Cassing and E. L. Bratkovskaya, Nucl. Phys. A **623** 570 (1997).
- [2] N. Armesto and A. Capella, Phys. Lett. B **430**, 23 (1998).
- [3] M. E. Peskin, Nucl. Phys. B **156**, 365 (1979).
- [4] G. Bhanot and M. E. Peskin, Nucl. Phys. B **156**, 391 (1979).
- [5] D. Kharzeev and H. Satz, Phys. Lett. B **334**, 155 (1994); D. Kharzeev *et al.*, *ibid.* **389**, 595 (1996).
- [6] F. Arleo *et al.*, Phys. Rev. D **65**, 014005 (2002).
- [7] Y. Oh, S. Kim, S. H. Lee, Phys. Rev. C **65**, 067901 (2002).
- [8] S. G. Matinyan and B. Muller, Phys. Rev. C **58**, 2994 (1998); K. L. Haglin, *ibid.* **61**, 031902(R) (2000); Z. Lin and C. M. Ko, *ibid.* **62**, 034903 (2000); Y. Oh, T. Song, and S. H. Lee, *ibid.* **63**, 034901 (2001); A. Sibirtsev, K. Tsushima, and A.W. Thomas, *ibid.* **63**, 044906 (2001).
- [9] W. Liu, C. M. Ko and Z. W. Lin, Phys. Rev. C **65**, 015203 (2001).
- [10] F. S. Navarra, M. Nielsen and M. R. Robilotta, Phys. Rev. C **64** 021901(R) (2001).
- [11] F. S. Navarra, M. Nielsen, R. S. Marques de Carvalho and G. Krein, Phys. Lett. B **529** 87 (2002); Francisco O. Duraes *et al.* nucl-th/0211092 and nucl-th/0210075.
- [12] C. Y. Wong, E. S. Swanson and T. Barnes, Phys. Rev. C **65**, 014903 (2002), Erratum-*ibid.* C **66**, 029901 (2002).
- [13] Z. W. Lin, C. M. Ko, and B. Zhang, Phys. Rev. C **61**, 024904 (2000).
- [14] Z. Lin, T. G. Di, and C. M. Ko, Nucl. Phys. A **689**, 965 (2001); Z. Lin, C. M. Ko, and B. Zhang, Phys. Rev. C **61**, 024904 (2000).
- [15] W. Liu and C. M. Ko, Phys. Lett. B **533** 259 (2002).
- [16] K. Abe *et al.* Phys. Rev. D **30**, 1 (1984).
- [17] See <http://jkj.tokai.jaeri.go.jp/>.
- [18] See <http://www.gsi.de/GSI-future>.
- [19] Chungsik Song, Phys. Rev. C **47**, 2861 (1993).
- [20] B. Holzenkamp, K. Holinde, and J. Speth, Nucl. Phys. A **500**, 485 (1989); G. Janssen, J.W. Durso, K. Holinde, B.C. Pearce, and J. Speth, Phys. Rev. Lett. **71**, 1978 (1993).
- [21] G. Janssen, K. Holinde, and J. Speth, Phys. Rev. C **54**, 2218 (1996).
- [22] F. S. Navarra, M. Nielsen, and M. E. Bracco, Phys. Rev. D **65** 037502 (2002).
- [23] T. Yao, Phys. Rev. **125**, 1048 (1961).

- [24] J. Vermaseren, computer code FORM, 1989. Free version of the software is available on the internet at <ftp://hep.itp.tuwien.ac.at/pub/FORM/PC/>.
- [25] S. Nozawa, B. Blankleider, T.-S.H.Lee, Nucl. Phys. A **513**, 459 (1990).
- [26] R. A. Adelseck and B. Saghai, Phys. Rev. C **42**, 108 (1990).
- [27] F. S. Navarra and M. Nielsen, Phys. Lett. B **433**, 285 (1998); F. O. Durães, F. S. Navarra, and M. Nielsen, *ibid.*, **498**, 169 (2001).
- [28] M. A. Shifman, A. I. Vainshtein, V. I. Zakharov, Phys. Lett. B **65**, 255 (1976), Nucl. Phys. B **136**, 125 (1978).
- [29] H. Fritzsch and K. H. Streng, Phys. Lett. B **72**, 385 (1978).
- [30] R.K. Ellis and P. Nason, Nucl. Phys. B **312**, 551 (1989).
- [31] <http://durpdg.dur.ac.uk/HEPDATA/PDF>.
- [32] S. Frixione, Nucl. Phys. Proc. Suppl. **79**, 399 (1999); hep-ph/9905545.

Charm production from photo-nucleon reaction in a hadronic model

W. Liu¹, S. H. Lee^{1,2}, and C. M. Ko¹

¹*Cyclotron Institute and Physics Department, Texas A&M University, College Station, Texas 77843-3366, USA*

²*Department of Physics and Institute of Physics and Applied Physics, Yonsei University, Seoul 120-749, Korea*

We study the total cross section for photo production of charmed hadrons near threshold using a hadronic Lagrangian. Both two-body final states involving Λ_c and a charmed meson as well as three-body final states involving nucleon and a charm-anticharm meson pair are included. With appropriate cut-off parameters in the form factors at interaction vertices, the model gives a total cross section that is consistent with the measured data at center-of-mass energy of 6 GeV. The result is compared with the prediction from the leading-order perturbative QCD.

PACS numbers: 25.75.-q, 13.75.Lb, 14.40.Gx, 14.40.Lb

I. INTRODUCTION

Reliable estimates of the production and scattering cross sections of open and/or hidden charmed hadrons in hadronic matter are important for understanding many phenomena in relativistic heavy ion collisions and hadron-nucleus reactions. In particular, the dissociation cross sections of J/ψ by light meson or nucleon are directly related to the role of hadronic suppression of J/ψ production in heavy ion collisions [1,2], and have thus been a subject under active investigations. In the heavy charm quark mass limit, a formula based on the leading-order (LO) perturbative QCD was derived in Refs. [3,4] for the absorption cross sections of J/ψ by hadrons. Higher-order corrections due to the target mass and relativistic effects have also been estimated [5–7]. However, the perturbative QCD approach is useful only at very high energy when nontrivial higher twist and higher α_s corrections are small. At low energies, these corrections become large, so nonperturbative approaches are needed. Various phenomenological models have thus been introduced for studying the J/ψ absorption cross section by hadrons at low energies. These include the hadronic model based on effective Lagrangians [8–10], the QCD sum rules [11], and the quark-exchange model [12]. Results from these phenomenological models all give much larger cross sections for J/ψ absorption by light mesons than that given by the perturbative QCD formula. To test the prediction from the hadronic model, the same effective Lagrangian has been used to evaluate the absorption cross section of J/ψ by nucleon, and it is found to be consistent with that extracted from photonuclear production of J/ψ [9].

In the present paper, we generalize the effective hadronic Lagrangian, which has also been used to study charmed meson scattering by hadrons [13,14] and charmed meson production from meson-nucleon scattering [15], to include the photon and to study charmed hadron production from photo-nucleon reaction near threshold. Both two-body ($\Lambda_c D$) and three-body ($N D \bar{D}$) final states are included. We find that using reasonable values for the cutoff parameters at the interaction vertices, the resulting charmed hadron production cross

section near threshold energy is consistent with the measured one at center-of-mass energy of 6 GeV [16], although at high energies its value is much smaller than that measured experimentally or given by the LO perturbative QCD. We further find that the relative contribution of two-body to three-body final states is also consistent with the experimental data. Our results thus provide another independent test and confirmation of the validity of hadronic model for determining the cross sections involving heavy flavors at low energies. The effective hadronic Lagrangian used in the present study will also be useful for evaluating other low energy cross sections involving heavy flavored hadrons, which can be studied at both the Japanese Hadron facility [17] and at the GSI future accelerator [18], where open and hidden charmed hadrons are copiously produced in proton- and antiproton-nucleus reactions near threshold.

This paper is organized as follows. In Section II, we first calculate the cross sections for photoproduction of charmed hadrons from nucleon with three particles in the final state, which is dominated by pion and rho meson exchange. Photoproduction of charmed hadrons from nucleon with two particle in the final state, which includes the charmed meson exchange, is studied in Section III. In Section IV, we show the total cross section and compare it to available experimental data and results from the LO QCD. Finally, summary and discussions are given in Section V.

II. PHOTOPRODUCTION OF CHARMED HADRONS FROM NUCLEON WITH THREE-PARTICLE FINAL STATES

In photoproduction of charmed hadrons from nucleon with three particle in the final states, the three possible reactions are $\gamma N \rightarrow \bar{D} D N$, $\gamma N \rightarrow \bar{D} D^* N (\bar{D}^* D N)$, and $\gamma N \rightarrow \bar{D}^* D^* N$. The lowest-order diagrams for the process $\gamma N \rightarrow \bar{D} D N$ are shown in Fig. 1 and involves the exchange of pion in the intermediate state; those for the processes $\gamma N \rightarrow \bar{D} D^* N (\bar{D}^* D N)$ and $\gamma N \rightarrow \bar{D}^* D^* N$ involve the exchange of rho meson, and the lowest-order diagrams for the two processes are shown in 2 and 3.

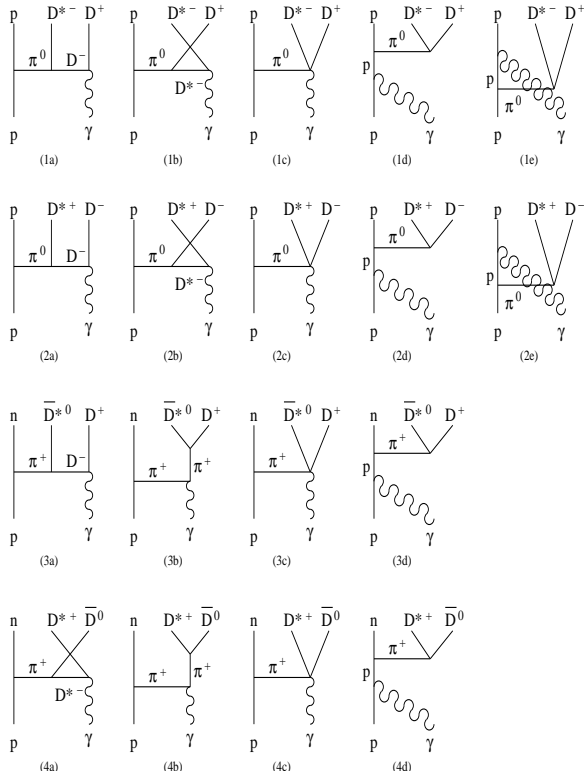


FIG. 1. Photoproduction of charmed hadrons from nucleon involving pion exchange.

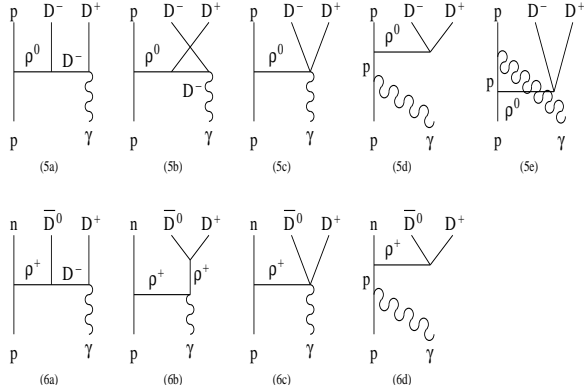


FIG. 2. Photoproduction of charmed hadrons ($D\bar{D}$) from proton involving rho meson exchange.

To evaluate the cross sections for these processes, we use the same Lagrangian introduced in Refs. [9,14,15] for studying charmed meson scattering by hadrons. This Lagrangian is based on the gauged SU(4) flavor symmetry but with empirical masses. The coupling constants are taken, if possible, from empirical information. Otherwise, the SU(4) relations are used to relate the unknown coupling constants to the known ones. Photon is then introduced in the Lagrangian via gauging its $U_{em}(1)$ part as in ref. [19].

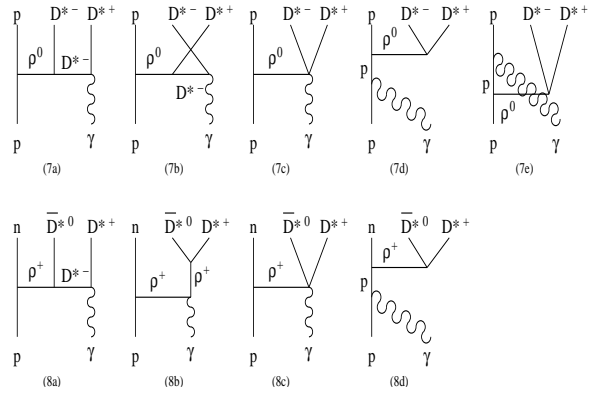


FIG. 3. Photoproduction of charmed hadrons ($D^*\bar{D}^*$) from proton involving rho meson exchange.

The interaction Lagrangian densities that are relevant to the processes shown in Figs. 1, 2, and 3 are given as follows:

$$\begin{aligned}
\mathcal{L}_{\pi NN} &= -ig_{\pi NN}\bar{N}\gamma_5\vec{\tau}N\cdot\vec{\pi}, \\
\mathcal{L}_{\rho NN} &= g_{\rho NN}\bar{N}\left(\gamma^\mu\vec{\tau}\cdot\vec{\rho}_\mu + \frac{\kappa_\rho}{2m_N}\sigma_{\mu\nu}\vec{\tau}\cdot\partial_\mu\vec{\rho}_\nu\right)N, \\
\mathcal{L}_{\pi DD^*} &= ig_{\pi DD^*}D^{*\mu}\vec{\tau}\cdot(\bar{D}\partial_\mu\vec{\pi} - \partial_\mu\bar{D}\vec{\pi}) + \text{H.c.}, \\
\mathcal{L}_{\rho DD} &= ig_{\rho DD}(D\vec{\tau}\partial_\mu\bar{D} - \partial_\mu D\vec{\tau}\bar{D})\cdot\vec{\rho}^\mu, \\
\mathcal{L}_{\rho D^*D^*} &= ig_{\rho D^*D^*}[(\partial_\mu D^{*\nu}\vec{\tau}\bar{D}_\nu^* - D^{*\nu}\vec{\tau}\partial_\mu\bar{D}_\nu^*)\cdot\vec{\rho}^\mu \\
&\quad + (D^{*\nu}\vec{\tau}\cdot\partial_\mu\vec{\rho}^\nu - \partial_\mu D^{*\nu}\vec{\tau}\cdot\vec{\rho}_\nu)\bar{D}^{*\mu} \\
&\quad + D^{*\mu}(\vec{\tau}\cdot\vec{\rho}^\nu\partial_\mu\bar{D}_\nu^* - \vec{\tau}\cdot\partial_\mu\vec{\rho}^\nu\bar{D}_\nu^*)], \\
\mathcal{L}_{\gamma DD} &= ieA^\mu[DQ\partial_\mu\bar{D} - (\partial_\mu D)Q\bar{D}], \\
\mathcal{L}_{\gamma D^*D^*} &= ie[A^\mu(\partial_\mu D^{*\nu}Q\bar{D}_\nu^* - D^{*\nu}Q\partial_\mu\bar{D}_\nu^*) \\
&\quad + (\partial_\mu A^\nu D_\nu^* - A^\nu\partial_\mu D_\nu^*)Q\bar{D}^{*\mu} \\
&\quad + D^{*\mu}Q(A^\nu\partial_\mu\bar{D}_\nu^* - \partial_\mu A^\nu\bar{D}_\nu^*)], \\
\mathcal{L}_{\pi\gamma DD^*} &= -eg_{\pi DD^*}A^\mu(D_\mu^*(2\vec{\tau}Q - Q\vec{\tau})\bar{D} \\
&\quad + D(2Q\vec{\tau} - \vec{\tau}Q)\bar{D}_\mu^*)\cdot\vec{\pi}, \\
\mathcal{L}_{\rho\gamma DD} &= eg_{\rho DD}A^\mu D(\vec{\tau}Q + Q\vec{\tau})\bar{D}\cdot\vec{\rho}_\mu, \\
\mathcal{L}_{\rho\gamma D^*D^*} &= eg_{\rho D^*D^*}(A^\nu D_\nu^*(2\vec{\tau}Q - Q\vec{\tau})\bar{D}_\mu^* \\
&\quad + A^\nu D_\mu^*(2\vec{\tau}Q - Q\vec{\tau})\bar{D}_\nu^* \\
&\quad - A_\mu D^{*\nu}(2\vec{\tau}Q - Q\vec{\tau})\bar{D}_\nu^*)\cdot\vec{\rho}^\mu. \tag{1}
\end{aligned}$$

In the above, $\vec{\tau}$ are Pauli spin matrices, and $\vec{\pi}$ and $\vec{\rho}$ denote the pion and rho meson isospin triplet, respectively, while $D = (D^0, D^+)$ and $D^* = (D^{*0}, D^{*+})$ denote the pseudoscalar and vector charm meson doublets, respectively. The operator Q is the diagonal charge operator with diagonal elements equal to 0 and -1.

For coupling constants in the above interaction Lagrangians, we use the following empirical values: $g_{\pi NN} = 13.5$ [20], $g_{\rho NN} = 3.25$, $\kappa_\rho = 6.1$ [21], $g_{\pi DD^*} = 5.56$ [15,22], and $g_{\rho DD} = 2.52$ [14].

The diagrams in Figs. 1, 2, and 3 can be separated to two types; one in which the photon is coupled to mesons such as the first three diagrams (denoted by (ia) to (ic) with $i=1$ to 8), and the other in which the photon is

coupled directly to the incoming or outgoing charged nucleon. As shown later, contributions from the latter type are much smaller than those from the first type of diagrams and are thus neglected in the following calculations. We note that diagrams of the first type are similar to those for J/ψ absorption on nucleon, which can be interpreted as absorption by the virtual pion and rho meson cloud of a nucleon. Here, they can be considered as charmed hadron production from the nucleon's virtual meson cloud.

The amplitudes for the four processes in Fig. 1 are given by

$$\mathcal{M}_i = -ia g_{\pi NN} \bar{N}(p_3) \gamma_5 N(p_1) \frac{1}{t - m_\pi^2} \times (M_{ia} + M_{ib} + M_{ic}), \quad (2)$$

with $i = 1$ to 4, while the amplitudes for the four processes in Fig. 2, 3 can be written as

$$\begin{aligned} \mathcal{M}_j &= a g_{\rho NN} \bar{N}(p_3) \left[\gamma^\mu + i \frac{\kappa_\rho}{2m_N} \sigma^{\alpha\mu} (p_1 - p_3)_\alpha \right] \\ &\times N(p_1) \left[-g_{\mu\nu} + \frac{(p_1 - p_3)_\mu (p_1 - p_3)_\nu}{m_\rho^2} \right] \\ &\times \frac{1}{t - m_\rho^2} (M_{ja}^\nu + M_{jb}^\nu + M_{jc}^\nu), \end{aligned} \quad (3)$$

with $j = 5$ to 8. In the above, p_1 and p_3 are four momenta of the initial and final nucleons, respectively. The coefficient a is, respectively, 1 and $\sqrt{2}$ for neutral and charged pion coupling to nucleon.

The three amplitudes M_{ia} , M_{ib} , and M_{ic} are for the subprocess $\pi\gamma \rightarrow D^* \bar{D}$ in Fig. 1. It can be shown that they fulfill the chiral constraint [10], i.e., their sum vanishes at the soft pion limit. Explicitly, they are given by

$$\begin{aligned} \mathcal{M}_{1a} &= \mathcal{M}_{2a} \\ &= e g_{\pi DD^*} (-2k_1 + k_3)^\mu \frac{1}{t - m_D^2} \\ &\times (k_1 - k_3 + k_4)^\nu \varepsilon_{3\mu} \varepsilon_{2\nu}, \\ \mathcal{M}_{1b} &= \mathcal{M}_{2b} \\ &= -e g_{\pi DD^*} (-k_1 - k_4)^\alpha \frac{1}{u - m_{D^*}^2} \\ &\times \left[g_{\alpha\beta} - \frac{(k_1 - k_4)_\alpha (k_1 - k_4)_\beta}{m_{D^*}^2} \right] \\ &\times [(-k_2 - k_3)^\beta g^{\mu\nu} + (-k_1 + k_2 + k_4)^\nu g^{\beta\mu} \\ &+ (k_1 + k_3 - k_4)^\mu g^{\beta\nu}] \varepsilon_{3\mu} \varepsilon_{2\nu}, \\ \mathcal{M}_{1c} &= \mathcal{M}_{2c} \\ &= e g_{\pi DD^*} g^{\mu\nu} \varepsilon_{3\mu} \varepsilon_{2\nu}, \\ \mathcal{M}_{3a} &= \sqrt{2} e g_{\pi DD^*} (-2k_1 + k_3)^\mu \frac{1}{t - m_D^2} \\ &\times (k_1 - k_3 + k_4)^\nu \varepsilon_{3\mu} \varepsilon_{2\nu}, \\ \mathcal{M}_{3b} &= -\sqrt{2} e g_{\pi DD^*} (2k_1 + k_2)^\nu \frac{1}{s - m_\pi^2} \end{aligned}$$

$$\begin{aligned} &\times (k_1 + k_2 + k_4)^\mu \varepsilon_{3\mu} \varepsilon_{2\nu}, \\ \mathcal{M}_{3c} &= 2\sqrt{2} e g_{\pi DD^*} g^{\mu\nu} \varepsilon_{3\mu} \varepsilon_{2\nu}, \\ \mathcal{M}_{4a} &= -\sqrt{2} e g_{\pi DD^*} (-k_1 - k_4)^\alpha \frac{1}{u - m_{D^*}^2} \\ &\times \left[g_{\alpha\beta} - \frac{(k_1 - k_4)_\alpha (k_1 - k_4)_\beta}{m_{D^*}^2} \right] \\ &\times [(-k_2 - k_3)^\beta g^{\mu\nu} + (-k_1 + k_2 + k_4)^\nu g^{\beta\mu} \\ &+ (k_1 + k_3 - k_4)^\mu g^{\beta\nu}] \varepsilon_{3\mu} \varepsilon_{2\nu}, \\ \mathcal{M}_{4b} &= \sqrt{2} e g_{\pi DD^*} (2k_1 + k_2)^\nu \frac{1}{s - m_\pi^2} \\ &\times (k_1 + k_2 + k_4)^\mu \varepsilon_{3\mu} \varepsilon_{2\nu}, \\ \mathcal{M}_{4c} &= -\sqrt{2} e g_{\pi DD^*} g^{\mu\nu} \varepsilon_{3\mu} \varepsilon_{2\nu}, \end{aligned} \quad (4)$$

where k_i denotes the momentum of particle i of each subprocess, and ε_μ and ε_ν are the polarization vector of γ and D^* , respectively. We choose the convention that particles 1 and 2 represent initial-state particles while particles 3 and 4 represent final-state ones on the left and right sides of the diagrams.

The amplitudes M_{ja}^ν , M_{jb}^ν , and M_{jc}^ν are those for the subprocesses $\rho\gamma \rightarrow D\bar{D}$ and $\rho\gamma \rightarrow D^* \bar{D}^*$ in Figs. 2 and 3, and they are written explicitly as:

$$\begin{aligned} \mathcal{M}_{5a}^\mu &= -e g_{\rho DD} (k_1 - 2k_3)^\mu \frac{1}{t - m_D^2} \\ &\times (k_1 - k_3 + k_4)^\nu \varepsilon_{2\nu}, \\ \mathcal{M}_{5b}^\mu &= -e g_{\rho DD} (-k_1 + 2k_4)^\mu \frac{1}{u - m_D^2} \\ &\times (-k_1 - k_3 + k_4)^\nu \varepsilon_{2\nu}, \\ \mathcal{M}_{5c}^\mu &= 2e g_{\rho DD} g^{\mu\nu} \varepsilon_{2\nu}, \\ \mathcal{M}_{6a}^\mu &= \sqrt{2} e g_{\rho DD} (k_1 - 2k_3)^\mu \frac{1}{t - m_D^2} \\ &\times (k_1 - k_3 + k_4)^\nu \varepsilon_{2\nu}, \\ \mathcal{M}_{6b}^\mu &= \sqrt{2} e g_{\rho DD} [(-2k_1 - k_2)^\nu g^{\mu\alpha} \\ &+ (k_1 + 2k_2)^\mu g^{\alpha\nu} + (k_1 - k_2)^\alpha g^{\mu\nu}] \frac{1}{s - m_\rho^2} \\ &\times \left[g_{\alpha\beta} - \frac{(k_1 + k_2)_\alpha (k_1 + k_2)_\beta}{m_\rho^2} \right] \\ &\times (k_3 - k_4)^\beta \varepsilon_{2\nu}, \\ \mathcal{M}_{6c}^\mu &= -\sqrt{2} e g_{\rho DD} g^{\mu\nu} \varepsilon_{2\nu}, \\ \mathcal{M}_{7a}^\mu &= e g_{\rho D^* D^*} [(-k_1 - k_3)^\alpha g^{\mu\lambda} + (2k_1 - k_3)^\lambda g^{\alpha\mu} \\ &+ (2k_3 - k_1)^\mu g^{\alpha\lambda}] \frac{1}{t - m_{D^*}^2} \\ &\times \left[g_{\alpha\beta} - \frac{(k_1 - k_3)_\alpha (k_1 - k_3)_\beta}{m_{D^*}^2} \right] \\ &\times [-2p_2^\omega g^{\beta\nu} + (k_2 + k_4)^\beta g^{\nu\omega} - 2k_4^\nu g^{\beta\omega}] \\ &\times \varepsilon_{2\nu} \varepsilon_{3\lambda} \varepsilon_{4\omega}, \\ \mathcal{M}_{7b}^\mu &= e g_{\rho D^* D^*} [(-2k_1 + k_4)^\omega g^{\alpha\mu} + (k_1 + k_4)^\alpha g^{\mu\omega} \end{aligned}$$

$$\begin{aligned}
& + (k_1 - 2k_4)^\mu g^{\alpha\omega}] \frac{1}{u - m_{D^*}^2} \\
& \times \left[g_{\alpha\beta} - \frac{(k_1 - k_4)_\alpha (k_1 - k_4)_\beta}{m_{D^*}^2} \right] \\
& \times [(-k_2 - k_3)^\beta g^{\nu\lambda} + 2k_2^\lambda g^{\beta\nu} + 2k_3^\nu g^{\beta\lambda}] \\
& \times \varepsilon_{2\nu} \varepsilon_{3\lambda} \varepsilon_{4\omega}, \\
\mathcal{M}_{7c}^\mu & = eg_{\rho D^* D^*} (g^{\mu\lambda} g^{\nu\omega} + g^{\mu\omega} g^{\nu\lambda} - 2g^{\mu\nu} g^{\lambda\omega}) \\
& \times \varepsilon_{2\nu} \varepsilon_{3\lambda} \varepsilon_{4\omega}, \\
\mathcal{M}_{8a}^\mu & = \sqrt{2} eg_{\rho D^* D^*} [(-k_1 - k_3)^\alpha g^{\mu\lambda} + (2p_1 - p_3)^\lambda g^{\alpha\mu} \\
& + (2k_3 - k_1)^\mu g^{\alpha\lambda}] \frac{1}{t - m_{D^*}^2} \\
& \times \left[g_{\alpha\beta} - \frac{(k_1 - k_3)_\alpha (k_1 - k_3)_\beta}{m_{D^*}^2} \right] \\
& \times [-2p_2^\omega g^{\beta\nu} + (k_2 + k_4)^\beta g^{\nu\omega} - 2k_4^\nu g^{\beta\omega}] \\
& \times \varepsilon_{2\nu} \varepsilon_{3\lambda} \varepsilon_{4\omega}, \\
\mathcal{M}_{8b}^\mu & = -\sqrt{2} eg_{\rho D^* D^*} [(-2k_1 - k_2)^\nu g^{\mu\alpha} + (k_1 + 2k_2)^\mu g^{\alpha\nu} \\
& + (k_1 - k_2)^\alpha g^{\mu\nu}] \frac{1}{s - m_\rho^2} \\
& \times \left[g_{\alpha\beta} - \frac{(k_1 + k_2)_\alpha (k_1 + k_2)_\beta}{m_\rho^2} \right] \\
& \times [-2k_4^\lambda g^{\beta\omega} + 2k_3^\omega g^{\beta\lambda} + (k_4 - k_3)^\beta g^{\lambda\omega}] \\
& \times \varepsilon_{2\nu} \varepsilon_{3\lambda} \varepsilon_{4\omega}, \\
\mathcal{M}_{8c}^\mu & = -\sqrt{2} eg_{\rho D^* D^*} (g^{\mu\lambda} g^{\nu\omega} - 2g^{\mu\omega} g^{\nu\lambda} + g^{\mu\nu} g^{\lambda\omega}) \\
& \times \varepsilon_{2\nu} \varepsilon_{3\lambda} \varepsilon_{4\omega}. \tag{5}
\end{aligned}$$

The cross sections for these reactions with three particles in the final state can be expressed in terms of the off-shell cross sections of the subprocesses involving two particles in the final state. Following the method of Ref. [23] for the reaction $NN \rightarrow N\Lambda K$, the spin-averaged differential cross section for the four reactions in Fig. 1 can be written as

$$\begin{aligned}
\frac{d\sigma_{\gamma N \rightarrow ND^* \bar{D}}}{dtds_1} & = \frac{ag_{\pi NN}^2}{32\pi^2 sp_c^2} k\sqrt{s_1}(-t) \frac{1}{(t - m_\pi^2)^2} \\
& \times \sigma_{\rho\gamma \rightarrow D^* \bar{D}}(s_1, t) |F(t)|^2, \tag{6}
\end{aligned}$$

while those for the two reactions in Fig. 2 are

$$\begin{aligned}
\frac{d\sigma_{\gamma N \rightarrow ND \bar{D}}}{dtds_1} & = \frac{3ag_{\rho NN}^2}{64\pi^2 sp_c^2} k\sqrt{s_1} \frac{1}{(t - m_\rho^2)^2} [4(1 + \kappa_\rho)^2 \\
& \times (-t - 2m_N^2) \kappa_\rho^2 \frac{(4m_N^2 - t)^2}{2m_N^2} + 4(1 + \kappa_\rho) \\
& \times \kappa_\rho(4m_N^2 - t)] \sigma_{\rho\gamma \rightarrow D \bar{D}}(s_1, t) |F(t)|^2. \tag{7}
\end{aligned}$$

In the above, p_c is the center-of-mass momentum of γ and N , t is the squared four momentum transfer, and s is the squared center-of-mass energy. The quantity s_1 and k are, respectively, the squared invariant mass and center-of-mass momentum of the π and γ in the subprocess $\gamma N \rightarrow D^* \bar{D}N$ or of the ρ and γ in the subprocesses

$\gamma N \rightarrow D \bar{D}N$ and $\gamma N \rightarrow D^* \bar{D}^*N$. Cross sections for these subprocesses are obtained from the amplitudes in Eqs.(4) and (5) using the software package FORM [24] to evaluate the summation over the polarizations of both initial and final particles. The differential cross sections for the two reactions $\gamma N \rightarrow D^* \bar{D}^*N$ in Fig. 3 are similar to those for $\gamma N \rightarrow D \bar{D}N$ with $\sigma_{\rho\gamma \rightarrow D \bar{D}}(s_1, t)$ replaced by $\sigma_{\rho\gamma \rightarrow D^* \bar{D}^*}(s_1, t)$.

We have introduced the form factors $F_{\pi NN}$ and $F_{\rho NN}$ at the πNN and ρNN vertices, respectively, to take into account the finite size of hadrons. As in Ref. [9], both are taken to have the following monopole form:

$$F(t) = \frac{\Lambda^2 - m^2}{\Lambda^2 - t}, \tag{8}$$

where m is the mass of the exchanged pion or rho meson, and Λ is a cutoff parameter. Following Ref. [9] we take $\Lambda_{\pi NN} = 1.3$ GeV and $\Lambda_{\rho NN} = 1.4$ GeV. We have also introduced a universal form factor at the strong interaction vertices in the $\pi\gamma \rightarrow D^*D$, $\rho\gamma \rightarrow DD$, and $\rho\gamma \rightarrow D^*D^*$ two-body subprocesses. Such a prescription guarantees the gauge invariance when all diagrams are included in each process [25]. The form factor we include here is of the following dipole form:

$$f(\mathbf{q}^2) = \left(\frac{\Lambda^2}{\Lambda^2 + \mathbf{q}^2} \right)^2, \tag{9}$$

with \mathbf{q} denoting the three momentum of photon in the center-of-mass system. We choose the cutoff parameter Λ to be 1.45 GeV to best reproduce the data. This form is also our default choice of form factors in this paper, unless stated otherwise.

The cross sections for charmed hadron production from neutron is the same as that from proton if we neglect diagrams involving photon coupling directly to proton. The isospin-averaged cross section for the reaction $\gamma N \rightarrow \bar{D}DN$ is thus given by the sum of the cross sections for the four processes in Fig. 1, which are obtained by integrating Eq.(6) over t and s_1 . Similarly, one can obtain from Eq.(7) the isospin averaged cross sections for the reactions $\gamma N \rightarrow \bar{D}D^*N(\bar{D}^*DN)$ and $\gamma N \rightarrow \bar{D}^*D^*N$, shown respectively, in Figs. 2 and 3. The results are shown in Fig. 4 by the solid, dotted, and dashed curves, respectively, for the reactions $\gamma N \rightarrow \bar{D}DN$, $\gamma N \rightarrow \bar{D}D^*N(\bar{D}^*DN)$ and $\gamma N \rightarrow \bar{D}^*D^*N$. It is seen that the reaction $\gamma N \rightarrow \bar{D}D^*N(\bar{D}^*DN)$ has the largest cross section with a peak value of about 40 nb, while the reaction $\gamma N \rightarrow \bar{D}DN$ has the smallest cross section of only about 1 nb. The larger cross sections for processes involving a charmed vector meson in the final state is due to the presence of interaction vertices with three vector mesons, which have a stronger momentum dependence than vertices with fewer number of vector mesons, leading thus to a larger strength at high energies.

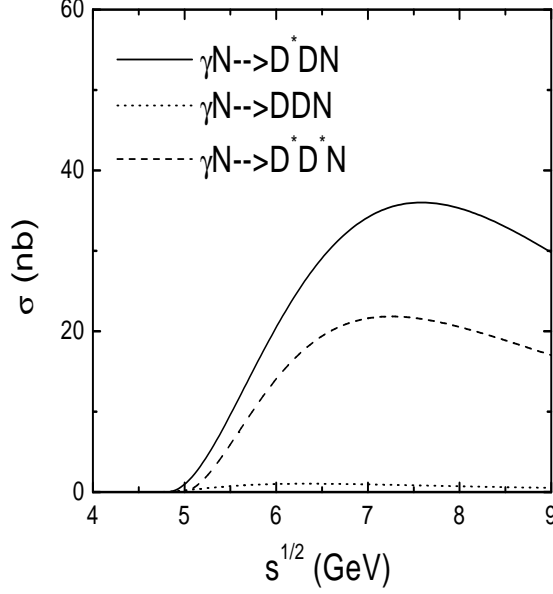


FIG. 4. Cross sections for photoproduction of charmed hadrons from nucleon with three particles in the final states.

The above results are obtained without contributions from diagrams involving the photon coupled directly to external nucleons. These diagrams are needed to preserve the gauge invariance in each process. Their contributions are small compared to those from diagrams with the photon coupled directly to mesons. This is due to the s -channel nucleon propagator ($1/(s - m_N^2)$) in these diagrams, which suppresses their amplitudes more than the t -channel heavy meson propagator in other as a result of the large photon energy needed to produce both the charmed and anticharmed meson pair. In the following, we demonstrate this effect by comparing the contribution due to diagram (1d) with that due to diagrams (1a)-(1c) in Fig. 1.

The amplitude for diagram (1d) in Fig. 1 can be written as

$$\begin{aligned} \mathcal{M} &= i2eg_{\pi NN}g_{\pi DD^*} \frac{1}{(s - m_N^2)(t - m_\pi^2)} \\ &\times \bar{p}(p_3)\gamma_5(\not{p}_1 + \not{p}_2 + m_N)\gamma^\mu p(p_1)\varepsilon_\mu p_5^\nu \varepsilon_\nu \\ &\equiv 2g_{\pi DD^*}M_2 p_5^\nu \varepsilon_\nu, \end{aligned} \quad (10)$$

where p_1 , p_3 , p_2 , and p_5 are the momenta of initial and final nucleons, photon, and charmed meson, respectively. The cross section due to this diagram alone is given by

$$\frac{d\sigma}{dtds_1} = \frac{\sqrt{s_1}}{256\pi^2 s p_c^2} |\mathcal{M}_2|^2 \Gamma(s_1), \quad (11)$$

where again p_c is the center-of-mass momentum of the nucleon and the photon, s_1 is the invariant mass of the $D^{*-}D^+$ pair, and $\Gamma(s_1)$ is the decay width of the off-shell $\pi^0 \rightarrow D^{*-}D^+$.

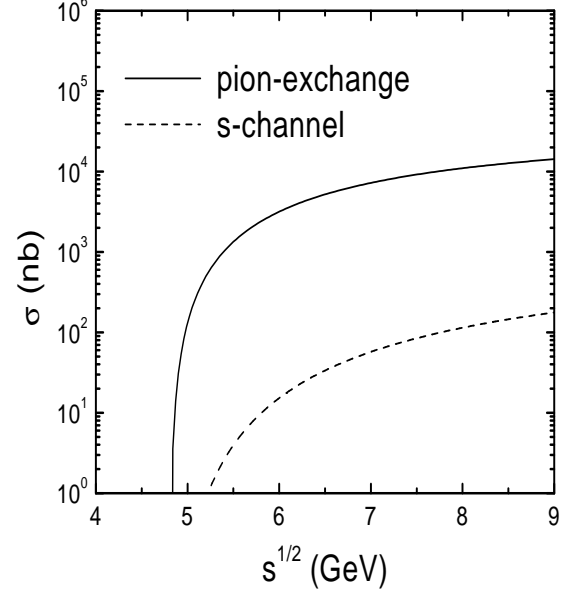


FIG. 5. Cross sections due to photon coupling directly to nucleon (diagram (1d) in Fig. 1, dashed curve) and due to pion exchange (diagrams (1a)-(1c) in Fig. 1, solid curve). No form factors are included at interaction vertices.

The cross section due to the s -channel diagram (1d) in Fig. 1 involving photon coupling directly to nucleon is shown by the dashed curve in Fig. 5 together with that coming from the pion exchange contributions (diagrams (1a)-(1c) in Fig. 1), shown by the solid curve. Form factors have been neglected in these results as we are only interested in their relative magnitude. It is seen that the contribution from the diagram with direct photon-nucleon coupling is more than two orders of magnitude smaller than that from the pion-exchange diagrams and can thus be safely neglected.

III. PHOTOPRODUCTION OF CHARMED HADRONS FROM NUCLEON WITH TWO-BODY FINAL STATES

Charmed hadron can also be produced in photon-nucleon reaction from processes involving two particles in the final state, i.e., $\gamma N \rightarrow \bar{D}\Lambda_c$ and $\gamma N \rightarrow \bar{D}^*\Lambda_c$, shown by diagrams in Fig. 6. The interaction Lagrangians needed to evaluate the cross sections for these reactions are:

$$\begin{aligned} \mathcal{L}_{DN\Lambda_c} &= ig_{DN\Lambda_c}(\bar{N}\gamma_5\Lambda_c\bar{D} + D\bar{\Lambda}_c\gamma_5 N), \\ \mathcal{L}_{D^*N\Lambda_c} &= g_{D^*N\Lambda_c}(\bar{N}\gamma_\mu\Lambda_c D^{*\mu} + \bar{D}^{*\mu}\bar{\Lambda}_c\gamma_\mu N). \end{aligned} \quad (12)$$

As in ref. [15], we use SU(4) relations to determine the coupling constants $g_{DN\Lambda_c}$ and $g_{D^*N\Lambda_c}$ in terms of known

coupling constants $g_{\pi NN}$ and $g_{\rho NN}$, and they are given by

$$g_{D N \Lambda_c} = \frac{3 - 2\alpha_D}{\sqrt{3}} g_{\pi NN} \simeq g_{\pi NN} = 13.5, \\ g_{D^* N \Lambda_c} = -\sqrt{3} g_{\rho NN} = -5.6, \quad (13)$$

where $\alpha_D = D/(D + F) \simeq 0.64$ [26] with D and F being the coefficients for the usual D -type and F -type couplings. Values of these couplings constants are similar to those obtained from a QCD sum rule analysis [27].

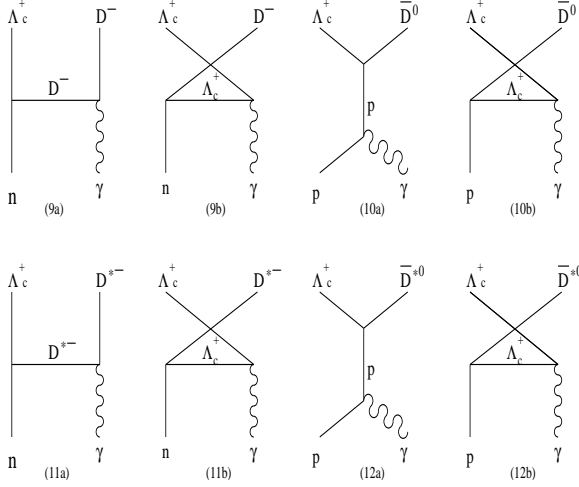


FIG. 6. Photoproduction of charmed hadrons from nucleon with two-particle final states.

The amplitudes for the two processes in Fig. 6 are

$$\begin{aligned} \mathcal{M}_9 &= (\mathcal{M}_{9a}^\mu + \mathcal{M}_{9b}^\mu) \varepsilon_\mu, \\ \mathcal{M}_{10} &= (\mathcal{M}_{10a}^\mu + \mathcal{M}_{10b}^\mu) \varepsilon_\mu, \\ \mathcal{M}_{11} &= (\mathcal{M}_{11a}^{\mu\nu} + \mathcal{M}_{11b}^{\mu\nu}) \varepsilon_\mu \varepsilon_\nu, \\ \mathcal{M}_{12} &= (\mathcal{M}_{12a}^{\mu\nu} + \mathcal{M}_{12b}^{\mu\nu}) \varepsilon_\mu \varepsilon_\nu, \end{aligned} \quad (14)$$

with \mathcal{M}_{9a}^μ , \mathcal{M}_{9b}^μ , \mathcal{M}_{10a}^μ , and \mathcal{M}_{10b}^μ for the top four diagrams in Fig. 6, while $\mathcal{M}_{11a}^{\mu\nu}$, $\mathcal{M}_{11b}^{\mu\nu}$, $\mathcal{M}_{12a}^{\mu\nu}$, and $\mathcal{M}_{12b}^{\mu\nu}$ for the bottom four diagrams. They are given explicitly by

$$\begin{aligned} \mathcal{M}_{9a}^\mu &= i e g_{D N \Lambda_c} \frac{1}{t - m_D^2} (p_2 - 2p_4)^\mu \bar{\Lambda}_c(p_3) \gamma^5 n(p_1), \\ \mathcal{M}_{9b}^\mu &= i e g_{D N \Lambda_c} \frac{1}{u - m_{\Lambda_c}^2} \\ &\quad \times \bar{\Lambda}_c(p_3) \gamma^\mu (\not{p}_1 - \not{p}_4 + m_{\Lambda_c}) \gamma^5 n(p_1), \\ \mathcal{M}_{10a}^\mu &= i e g_{D N \Lambda_c} \frac{1}{s - m_N^2} \\ &\quad \times \bar{\Lambda}_c(p_3) \gamma^5 (\not{p}_1 + \not{p}_2 + m_N) \gamma^\mu p(p_1), \\ \mathcal{M}_{10b}^\mu &= i e g_{D N \Lambda_c} \frac{1}{u - m_{\Lambda_c}^2} \\ &\quad \times \bar{\Lambda}_c(p_3) \gamma^\mu (\not{p}_1 - \not{p}_4 + m_{\Lambda_c}) \gamma^5 p(p_1), \end{aligned}$$

$$\begin{aligned} \mathcal{M}_{11a}^{\mu\nu} &= e g_{D^* N \Lambda_c} \bar{\Lambda}_c(p_3) \gamma^\alpha n(p_1) \frac{1}{t - m_{D^*}^2} \\ &\quad \times \left[-g_{\alpha\beta} + \frac{(p_1 - p_3)_\alpha (p_1 - p_3)_\beta}{m_{D^*}^2} \right] \\ &\quad \times [2p_2^\nu g^{\beta\mu} - (p_2 + p_4)^\beta g^{\mu\nu} + 2p_4^\mu g^{\beta\nu}], \\ \mathcal{M}_{11b}^{\mu\nu} &= e g_{D^* N \Lambda_c} \frac{1}{u - m_{\Lambda_c}^2} \\ &\quad \times \bar{\Lambda}_c(p_3) \gamma^\mu (\not{p}_1 - \not{p}_4 + m_{\Lambda_c}) \gamma^\nu n(p_1), \\ \mathcal{M}_{12a}^{\mu\nu} &= e g_{D^* N \Lambda_c} \frac{1}{s - m_N^2} \\ &\quad \times \bar{\Lambda}_c(p_3) \gamma^\nu (\not{p}_1 + \not{p}_2 + m_N) \gamma^\mu p(p_1), \\ \mathcal{M}_{12b}^{\mu\nu} &= e g_{D^* N \Lambda_c} \frac{1}{u - m_{\Lambda_c}^2} \\ &\quad \times \bar{\Lambda}_c(p_3) \gamma^\mu (\not{p}_1 - \not{p}_4 + m_{\Lambda_c}) \gamma^\nu p(p_1). \end{aligned} \quad (15)$$

Here, p_1 , p_2 , p_3 , and p_4 denote the momentum of γ , N , $\bar{D}(\bar{D}^*)$, and Λ_c , respectively.

The spin-averaged differential cross sections for the four processes in Fig. 6 are then

$$\frac{d\sigma_{\gamma N \rightarrow \bar{D} \Lambda_c}}{dt} = \frac{1}{256\pi s p_c^2} |\mathcal{M}_i|^2 |f(\mathbf{q}^2)|^2, \quad (16)$$

where $i = 9, 10, 11, 12$ for the the four reactions $\gamma n \rightarrow D^- \Lambda_c^+$, $\gamma p \rightarrow \bar{D}^0 \Lambda_c^+$, $\gamma n \rightarrow D^{*-} \Lambda_c^+$, and $\gamma \rightarrow D^- \Lambda_c^+$.

The isospin-averaged cross sections for the two reactions $\gamma N \rightarrow \bar{D} \Lambda_c$ and $\gamma N \rightarrow \bar{D}^* \Lambda_c$ can be obtained from the above cross sections, and they are given by

$$\begin{aligned} \sigma_{\gamma N \rightarrow \bar{D} \Lambda_c} &= \frac{1}{2} (\sigma_{\gamma n \rightarrow D^- \Lambda_c^+} + \sigma_{\gamma p \rightarrow \bar{D}^0 \Lambda_c^+}), \\ \sigma_{\gamma N \rightarrow \bar{D}^* \Lambda_c} &= \frac{1}{2} (\sigma_{\gamma n \rightarrow D^{*-} \Lambda_c^+} + \sigma_{\gamma p \rightarrow \bar{D}^{*0} \Lambda_c^+}). \end{aligned} \quad (17)$$

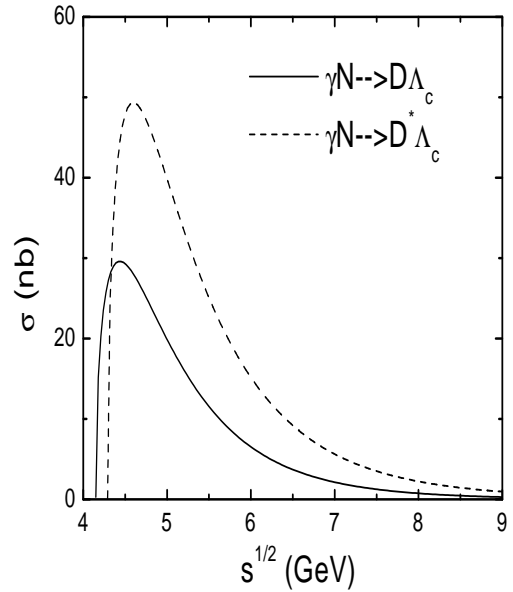


FIG. 7. cross section photoproduction of charmed hadrons via charmed meson exchange.

Taking the form factor at interaction vertices to be of the dipole type as in Eq. (9) and with a cutoff parameter $\Lambda = 1.45$ GeV, which is chosen to reproduce the experimentally observed relative strength between two-body and three-body decay final states in photoproduction of charmed hadrons on nucleon [16], the cross sections for the reactions $\gamma N \rightarrow \bar{D}\Lambda_c$ (dashed curve) and $\gamma N \rightarrow \bar{D}^*\Lambda_c$ (solid curve) are shown in Fig. 7 as functions of total center-of-mass energy. It is seen that both cross sections are large with a peak value of about 30 nb for $\gamma N \rightarrow \bar{D}\Lambda_c$ and about 50 nb for $\gamma N \rightarrow \bar{D}^*\Lambda_c$.

IV. TOTAL CROSS SECTION FOR CHARMED HADRON PRODUCTION IN PHOTON-NUCLEON REACTION

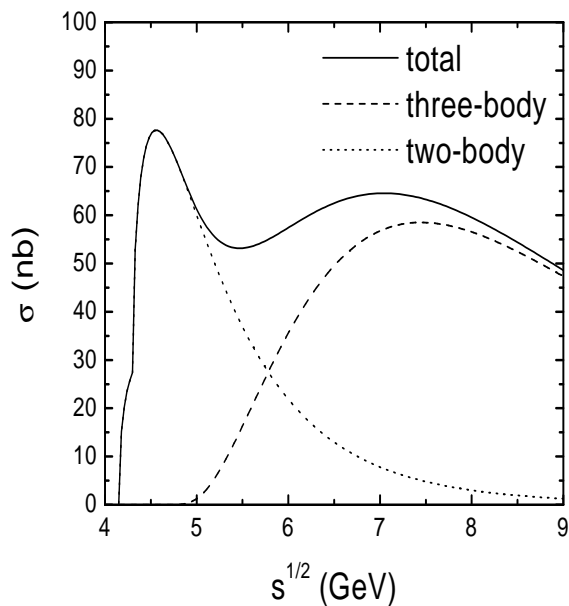


FIG. 8. Total and partial cross sections for charmed hadron production in photon-nucleon reactions as functions of center-of-mass energy.

The total cross section for photoproduction of charmed hadrons on nucleon is given by the sum of the cross sections for two-body and three-body final states. In Fig. 8, we show the total cross section (solid curve) together with that for two-body final state (dotted curve) and three-body final state (dashed curve). It is seen that two-body final states involving Λ_c and a charmed meson dominates at low energy, while the three-body final state involving a nucleon as well as a charmed and anticharmed meson pair is more important at high energies. The two have

comparable magnitudes around center-of-mass energy of about 5.7 GeV. This is consistent with the experimental data at 6 GeV [16], which shows that the final state with a Λ_c constitutes about 35% of the total cross section.

Charm production from photo-nucleon reaction can be estimated using the leading-order perturbative QCD [28–30]. The cross section in this approach is given by

$$\sigma^{\gamma N}(\nu) = \int_{2m_c^2/\nu}^1 dx \sigma^{\gamma g}(\nu x)g(x), \quad (18)$$

where m_c is the charm quark mass, $g(x)$ is the gluon distribution function inside the nucleon, and $\nu = p \cdot p_\gamma$ with p and p_γ being the momenta of the incoming nucleon and photon. The cross section $\sigma^{\gamma g}(\omega)$ is that for charm-anticharm quark production from the leading order photon-gluon scattering, i.e.,

$$\begin{aligned} \sigma^{\gamma g \rightarrow \bar{c}c}(\omega) = & \frac{2\pi\alpha_s\alpha}{9} \frac{4}{\omega^2} \left[\left(1 + \frac{4m_c^2}{\omega^2} - \frac{8m_c^2}{\omega^4} \right) \right. \\ & \times \log \frac{1 + \sqrt{1 - \frac{4m_c^2}{\omega^2}}}{1 + \sqrt{1 - \frac{4m_c^2}{\omega^2}}} \\ & \left. - \left(1 + \frac{4m_c^2}{\omega^2} \right) \sqrt{1 - \frac{4m_c^2}{\omega^2}} \right], \quad (19) \end{aligned}$$

where $\omega^2 = 2p_g \cdot p_\gamma$, with the gluon momentum denoted by p_g .

Using $m_c = 1.3$ GeV and the leading order MRST 2001 parameterization of the gluon distribution function in nucleon [31], we have calculated the photo charm production cross section on nucleon using the LO QCD formula, and the result is shown Fig. 9 by the dashed curve together with that from the effective hadronic model (solid curve) and the available experimental data (open circles). We see that the LO QCD result reproduces the data at 6 GeV and at higher energies. However, the QCD prediction below 6 GeV falls well below the results from the effective hadronic model. It is known that the QCD formula for photoproduction of heavy quarks should work best when the momenta involved are of order the heavy quark mass m_c . Below this momentum and near the threshold energy, large logarithms will appear in the perturbative QCD approach and spoil its convergence [32]. At these energies, our phenomenological hadronic approach should be more reliable as the cross section is dominated by two-body final states with no additional contribution to cause any large correction. On the other hand, the results from the hadronic model at higher energies fall short of the experimental data. This is expected because at these energies, contributions from four-body final state and from the exchange of heavier mesons will become important. At these higher energies, perturbative QCD calculations should be a more efficient way for determining the cross section for photo charm production than adding new ingredients into our phenomenological hadronic model.

ACKNOWLEDGMENT

This paper is based on work supported by the National Science Foundation under Grant No. PHY-0098805 and the Welch Foundation under Grant No. A-1358. SHL is also supported in part by the KOSEF under Grant No. 1999-2-111-005-5 and by the Korea Research Foundation under Grant No. KRF-2002-015-CP0074.

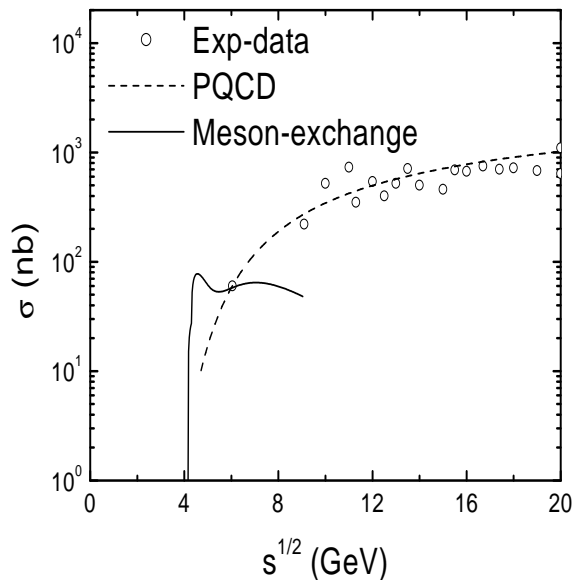


FIG. 9. Cross sections for charm production in photo nucleon reaction in the hadronic model (solid curve) and the pQCD approach (dashed curve). The experimental data are shown by open circles.

V. SUMMARY AND DISCUSSIONS

In summary, the total cross section for charmed hadron production in photo-nucleon reaction is evaluated in an effective hadronic model. This model is based on a gauged SU(4) flavor symmetric Lagrangian with the photon introduced as a $U_{em}(1)$ gauged particle. The symmetry breaking effect is taken into account via using empirical hadron masses and coupling constants. Form factors of the monopole type are introduced at interaction vertices. This hadronic model has been previously used to evaluate the dissociation cross section of J/ψ by hadrons. For photo production of charmed hadrons on nucleon, we have included both two-body final states involving a Λ_c and a charmed meson as well as three-body final states involving a nucleon and a charmed and anticharmed meson pair. It is found that reactions with two-body final states dominate the production cross section at low center-of-mass energies while reactions with three-body states are more important at high center-of-mass energies. Using cut-off parameters in the form factors from previous studies of J/ψ absorption by hadrons, the model reproduces the lowest available experimental data at center-of-mass energy of 6 GeV. Our results thus again confirm the validity of the effective hadron model in previous studies and provide a useful model for further studies of reactions involving heavy quarks at low and near threshold energies.

- [1] W. Cassing and C. M. Ko, Phys. Lett. B **396**, 39 (1997); W. Cassing and E. L. Bratkovskaya, Nucl. Phys. A **623** 570 (1997).
- [2] N. Armesto and A. Capella, Phys. Lett. B **430**, 23 (1998).
- [3] M. E. Peskin, Nucl. Phys. B **156**, 365 (1979).
- [4] G. Bhanot and M. E. Peskin, Nucl. Phys. B **156**, 391 (1979).
- [5] D. Kharzeev and H. Satz, Phys. Lett. B **334**, 155 (1994); D. Kharzeev *et al.*, *ibid.* **389**, 595 (1996).
- [6] F. Arleo *et al.*, Phys. Rev. D **65**, 014005 (2002).
- [7] Y. Oh, S. Kim, S. H. Lee, Phys. Rev. C **65**, 067901 (2002).
- [8] S. G. Matinyan and B. Muller, Phys. Rev. C **58**, 2994 (1998); K. L. Haglin, *ibid.* **61**, 031902(R) (2000); Z. Lin and C. M. Ko, *ibid.* **62**, 034903 (2000); Y. Oh, T. Song, and S. H. Lee, *ibid.* **63**, 034901 (2001); A. Sibirtsev, K. Tsushima, and A.W. Thomas, *ibid.* **63**, 044906 (2001).
- [9] W. Liu, C. M. Ko and Z. W. Lin, Phys. Rev. C **65**, 015203 (2001).
- [10] F. S. Navarra, M. Nielsen and M. R. Robilotta, Phys. Rev. C **64** 021901(R) (2001).
- [11] F. S. Navarra, M. Nielsen, R. S. Marques de Carvalho and G. Krein, Phys. Lett. B **529** 87 (2002); Francisco O. Duraes *et al.* nucl-th/0211092 and nucl-th/0210075.
- [12] C. Y. Wong, E. S. Swanson and T. Barnes, Phys. Rev. C **65**, 014903 (2002), Erratum-*ibid.* C **66**, 029901 (2002).
- [13] Z. W. Lin, C. M. Ko, and B. Zhang, Phys. Rev. C **61**, 024904 (2000).
- [14] Z. Lin, T. G. Di, and C. M. Ko, Nucl. Phys. A **689**, 965 (2001); Z. Lin, C. M. Ko, and B. Zhang, Phys. Rev. C **61**, 024904 (2000).
- [15] W. Liu and C. M. Ko, Phys. Lett. B **533** 259 (2002).
- [16] K. Abe *et al.* Phys. Rev. D **30**, 1 (1984).
- [17] See <http://jkj.tokai.jaeri.go.jp/>.
- [18] See <http://www.gsi.de/GSI-future>.
- [19] Chungsik Song, Phys. Rev. C **47**, 2861 (1993).
- [20] B. Holzenkamp, K. Holinde, and J. Speth, Nucl. Phys. A **500**, 485 (1989); G. Janssen, J.W. Durso, K. Holinde, B.C. Pearce, and J. Speth, Phys. Rev. Lett. **71**, 1978 (1993).
- [21] G. Janssen, K. Holinde, and J. Speth, Phys. Rev. C **54**, 2218 (1996).
- [22] F. S. Navarra, M. Nielsen, and M. E. Bracco, Phys. Rev. D **65** 037502 (2002).
- [23] T. Yao, Phys. Rev. **125**, 1048 (1961).

- [24] J. Vermaseren, computer code FORM, 1989. Free version of the software is available on the internet at <ftp://hep.itp.tuwien.ac.at/pub/FORM/PC/>.
- [25] S. Nozawa, B. Blankleider, T.-S.H.Lee, Nucl. Phys. A **513**, 459 (1990).
- [26] R. A. Adelseck and B. Saghai, Phys. Rev. C **42**, 108 (1990).
- [27] F. S. Navarra and M. Nielsen, Phys. Lett. B **433**, 285 (1998); F. O. Durães, F. S. Navarra, and M. Nielsen, *ibid.*, **498**, 169 (2001).
- [28] M. A. Shifman, A. I. Vainshtein, V. I. Zakharov, Phys. Lett. B **65**, 255 (1976), Nucl. Phys. B **136**, 125 (1978).
- [29] H. Fritzsch and K. H. Streng, Phys. Lett. B **72**, 385 (1978).
- [30] R.K. Ellis and P. Nason, Nucl. Phys. B **312**, 551 (1989).
- [31] <http://durpdg.dur.ac.uk/HEPDATA/PDF>.
- [32] S. Frixione, Nucl. Phys. Proc. Suppl. **79**, 399 (1999); hep-ph/9905545.